Supporting Information

for

Design, synthesis, and redox properties of ferrocene-functionalized phenothiazine and phenothiazine sulfone isomers

*Nikhil Ji Tiwari and Rajneesh Misra**

Department of Chemistry,

Indian Institute of Technology Indore, Indore-453552, India

Email: rajneeshmisra@iiti.ac.in

*Corresponding author

Experimental Details

Chemicals were used as received unless otherwise indicated. All the oxygen- or moisture-sensitive reactions were carried out under an argon atmosphere, and the reflux reactions were performed in an oil bath. ^{1}H NMR (400 MHz or 500 MHz) spectra were recorded on a Bruker 400 MHz FT-NMR or Bruker 500 MHz FT-NMR spectrometer at room temperature. Chemical shifts are reported in delta (δ) units, expressed in parts per million (ppm) downfield from tetramethylsilane (TMS) using the residual protonated solvent as an internal standard {$CDCl_3$, 7.26 ppm}. The Multiplicities are given as s (singlet), d (doublet), t (triplet) and m (multiplet) and the coupling constants, J, are given in hertz. ^{13}C NMR (100 MHz and 125 MHz) on a Bruker 400 MHz FT-NMR or Bruker 500 MHz FT-NMR spectrometer at room temperature. Chemical shifts are reported in delta (δ) un its, expressed in parts per million (ppm) downfield from TMS using the solvent as internal standard {$CDCl_3$, 77.16 ppm}. Thermogravimetric analysis was performed on the Mettler Toledo thermal analysis system. UV-visible absorption spectra of all compounds were recorded on a PerkinElmer Lambda 35 instrument in the DCM solution. All the measurements were carried out at 25 °C. HRMS were recorded on a Bruker-Daltonics micrOTOF-Q II mass spectrometer. The cyclic and differential pulse voltammograms (CVs and DPVs) were recorded on a PalmSens 4 electrochemical analyzer in the DCM solvent using glassy carbon as a working electrode, Pt wire as the counter electrode, and Ag/AgCl as the reference electrode. The scan rate was 100 mV s^{-1} for CV. A solution of tetrabutylammonium hexafluorophosphate ($TBAPF_6$) in DCM (0.1 M) was used as the supporting electrolyte. Spectroelectrochemical measurements were done using a commercially available platinum honeycomb working electrode on a ceramic support in a narrow optical path quartz cuvette using a miniature Ag/AgCl gel electrode as a reference electrode. The potential was controlled and switched with a potentiostat. The resulting spectroscopic changes were measured with ALS SEC2020 spectrometer system. DFT calculations were performed using the B3LYP/6-31G(d,p) (B3LYP functional with the 6-31G(d,p) basis set) for C, H, S, O, and N atoms, and the LanL2DZ basis set for the Fe atom.[1] Additionally, time-dependent DFT (TDDFT) calculations were conducted at the B3LYP/6-31G(d,p) level on the optimized structures in dichloromethane.[1]

Molecular Structure:

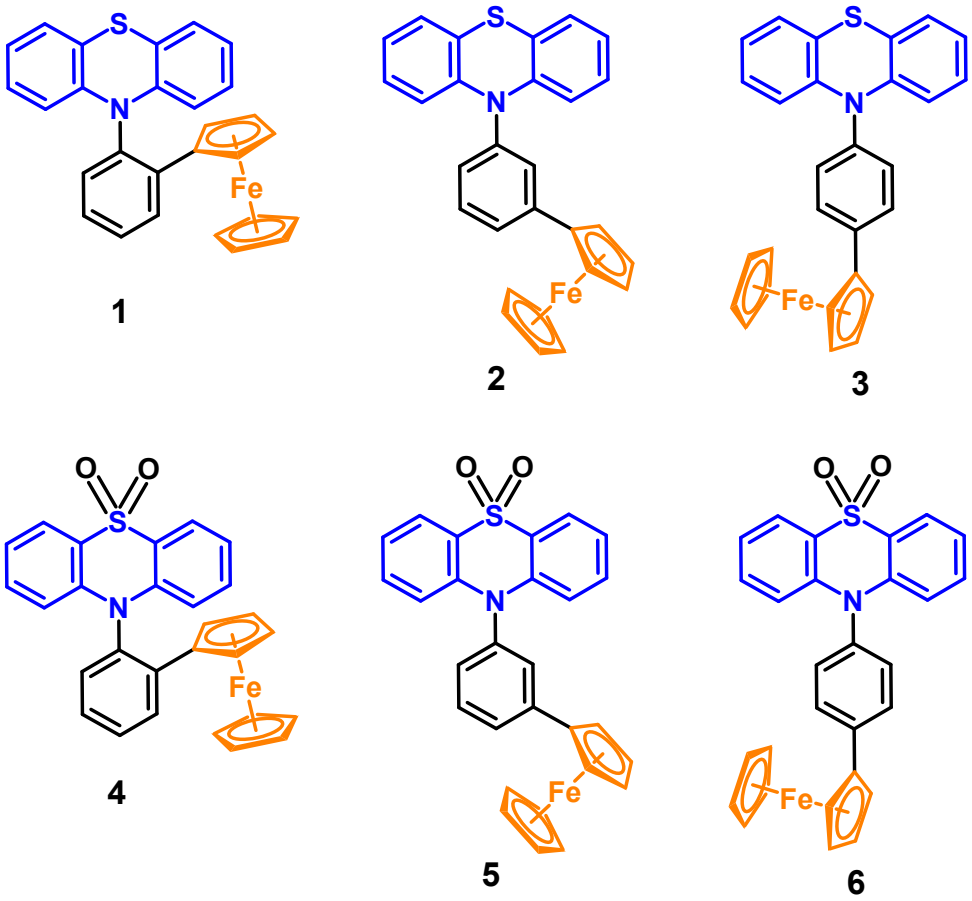

Chart S1. Molecular structures of ferrocenyl functionalized phenothiazine and phenothiazine sulfone derivatives **1–6**.

Synthetic Scheme:

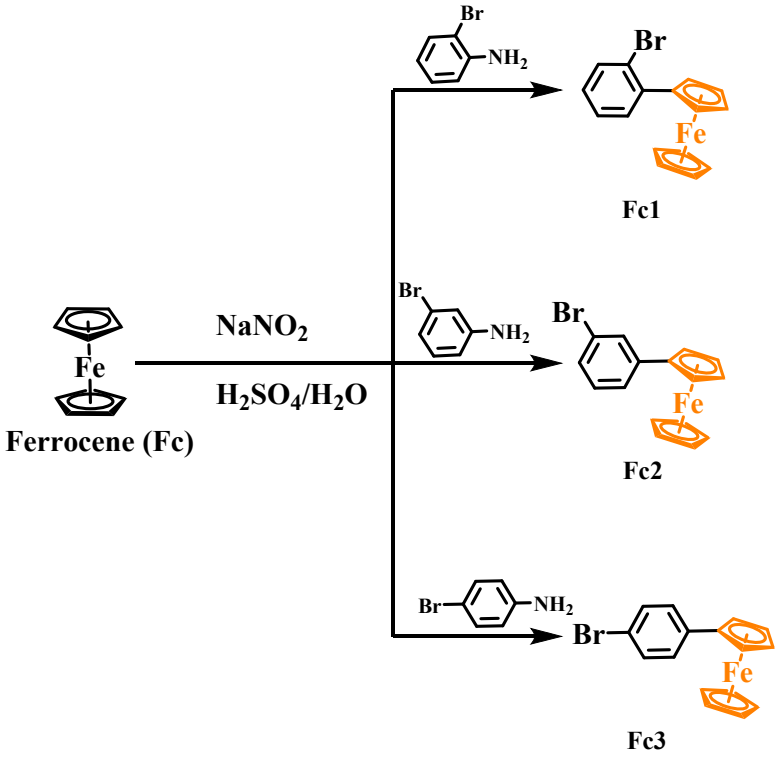

Scheme S1. Synthetic route to bromo derivatives of phenylene-linked ferrocene (**Fc1**, **Fc2**, and **Fc3**).

Theoretical Calculations:

(a) 1

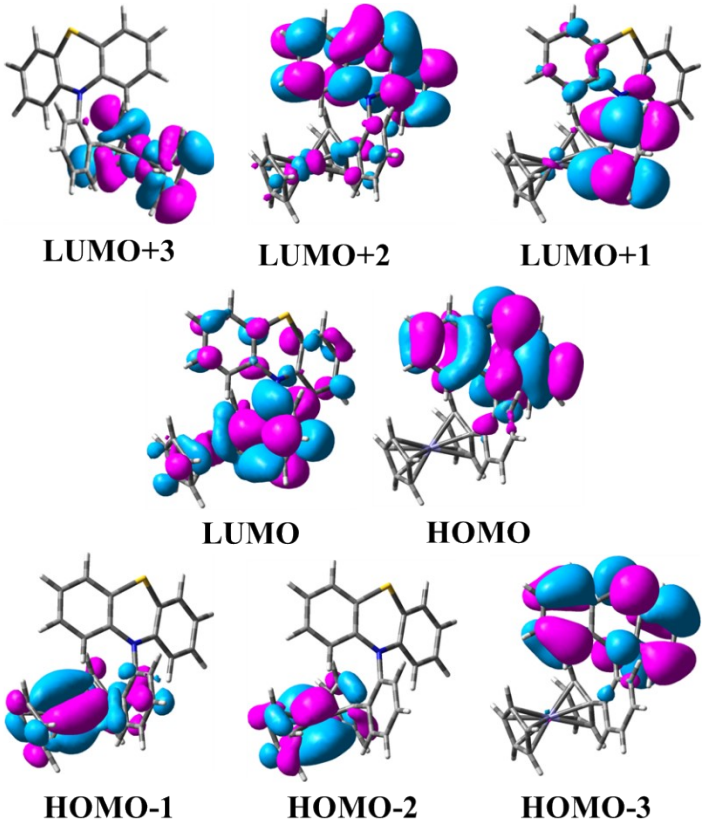

(b) 2

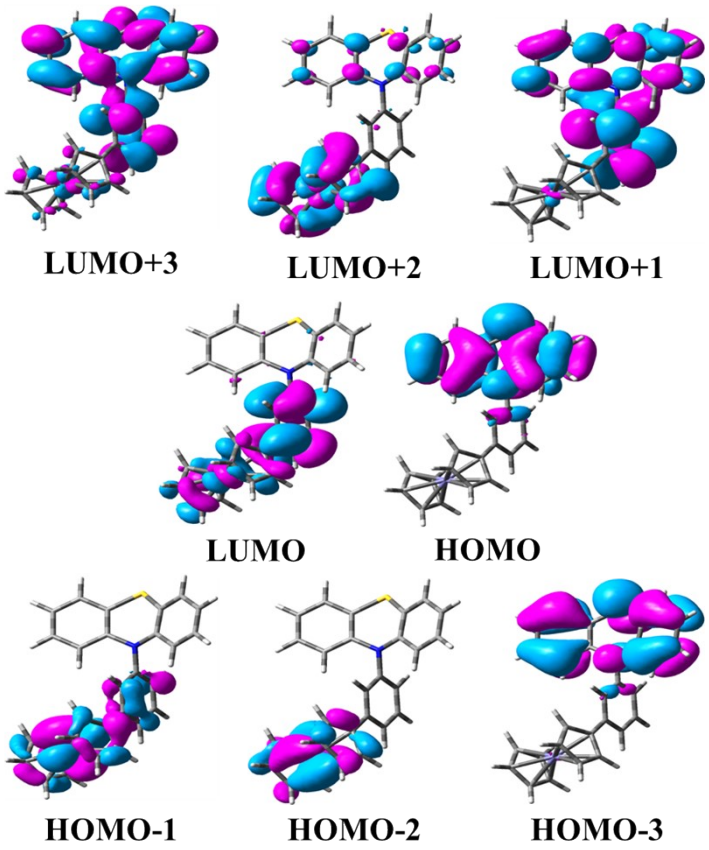

(c) 3

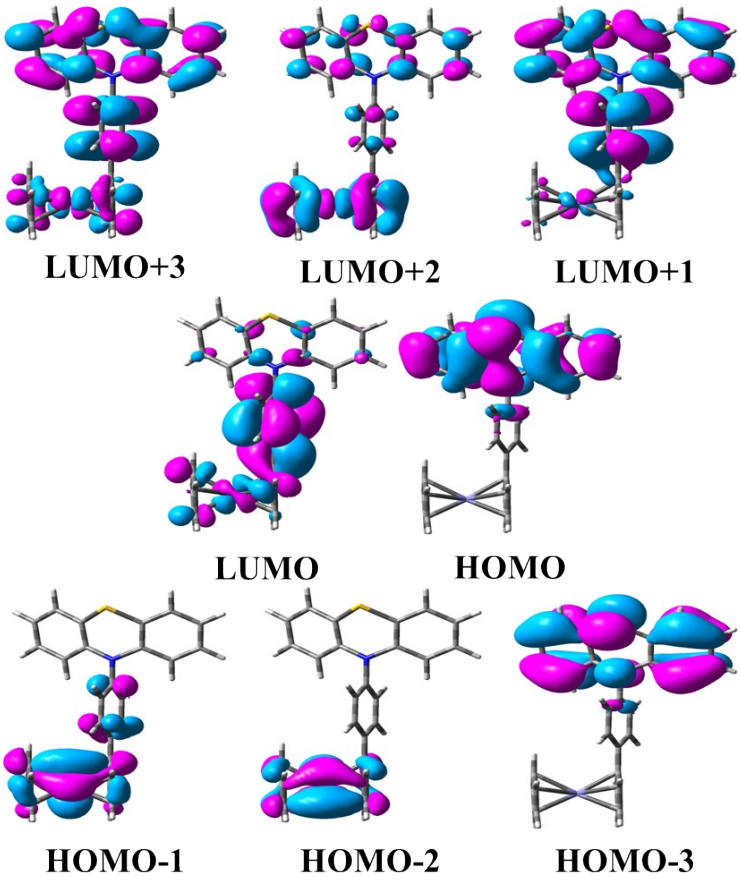
LUMO+3
LUMO+2
LUMO+1
LUMO
HOMO
HOMO-1
HOMO-2
HOMO-3

(d) 4

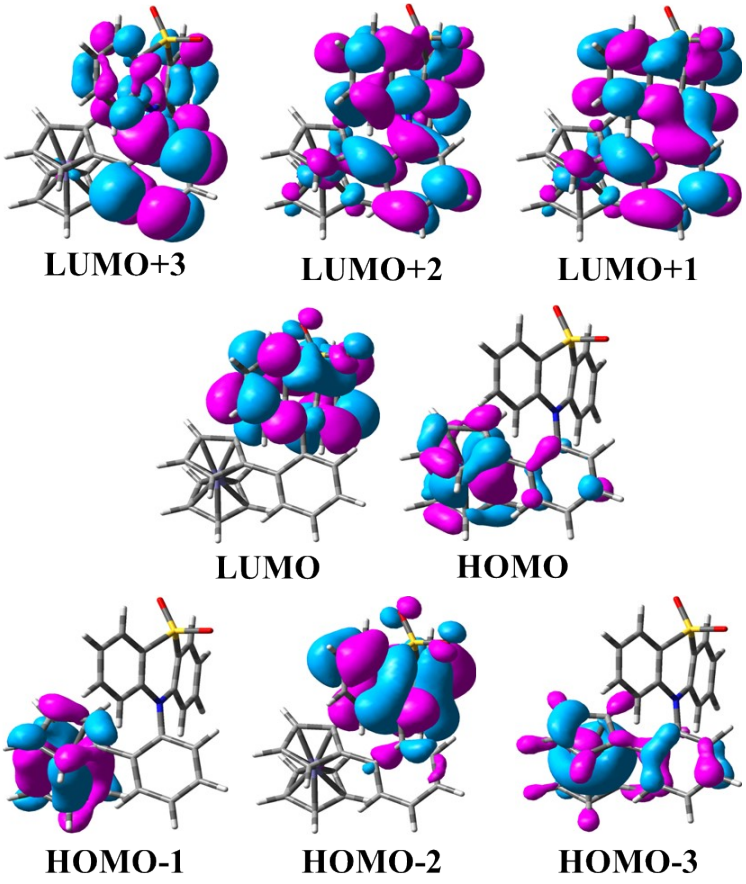
LUMO+3
LUMO+2
LUMO+1
LUMO
HOMO
HOMO-1
HOMO-2
HOMO-3

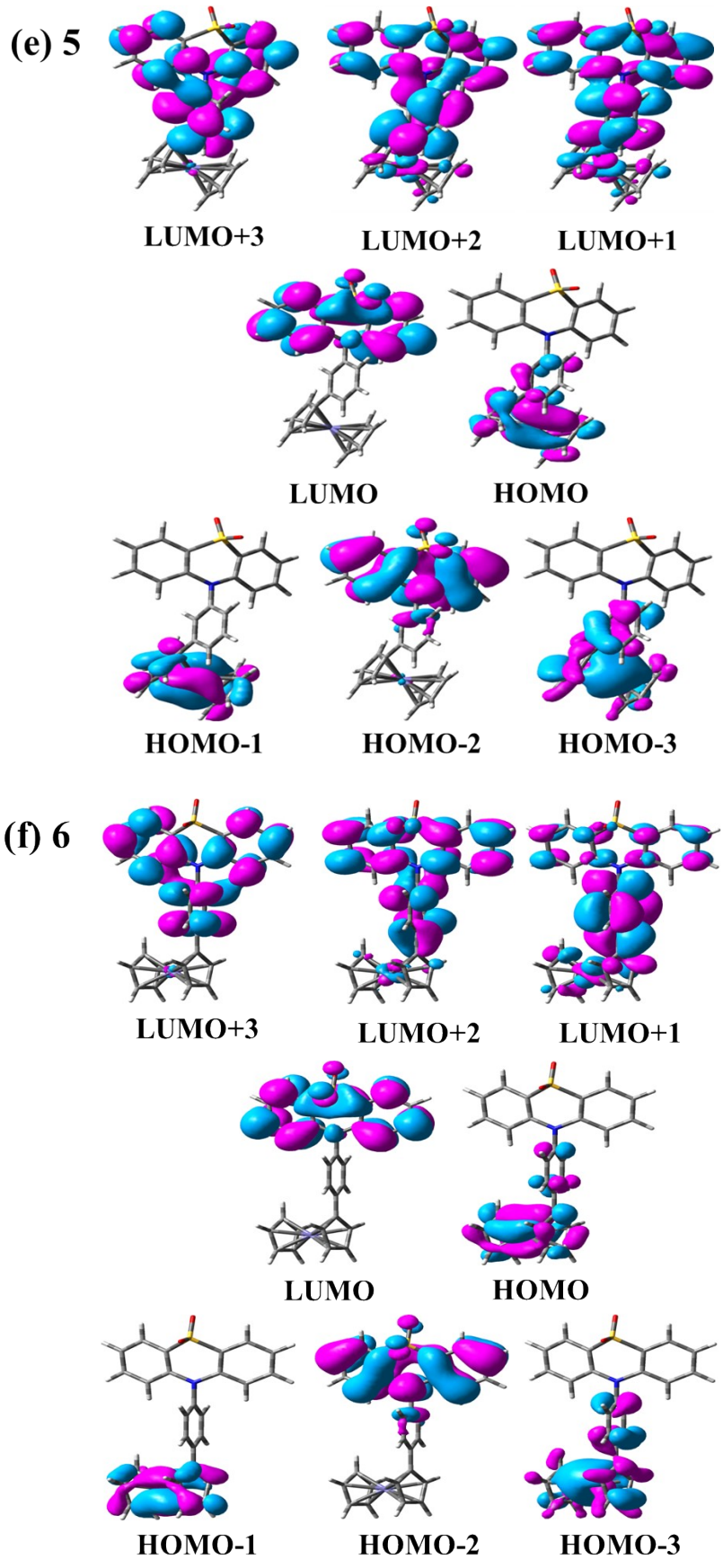

Fig. S1. The molecular orbitals of **1–6** estimated from DFT calculation.

Theoretical Calculations:

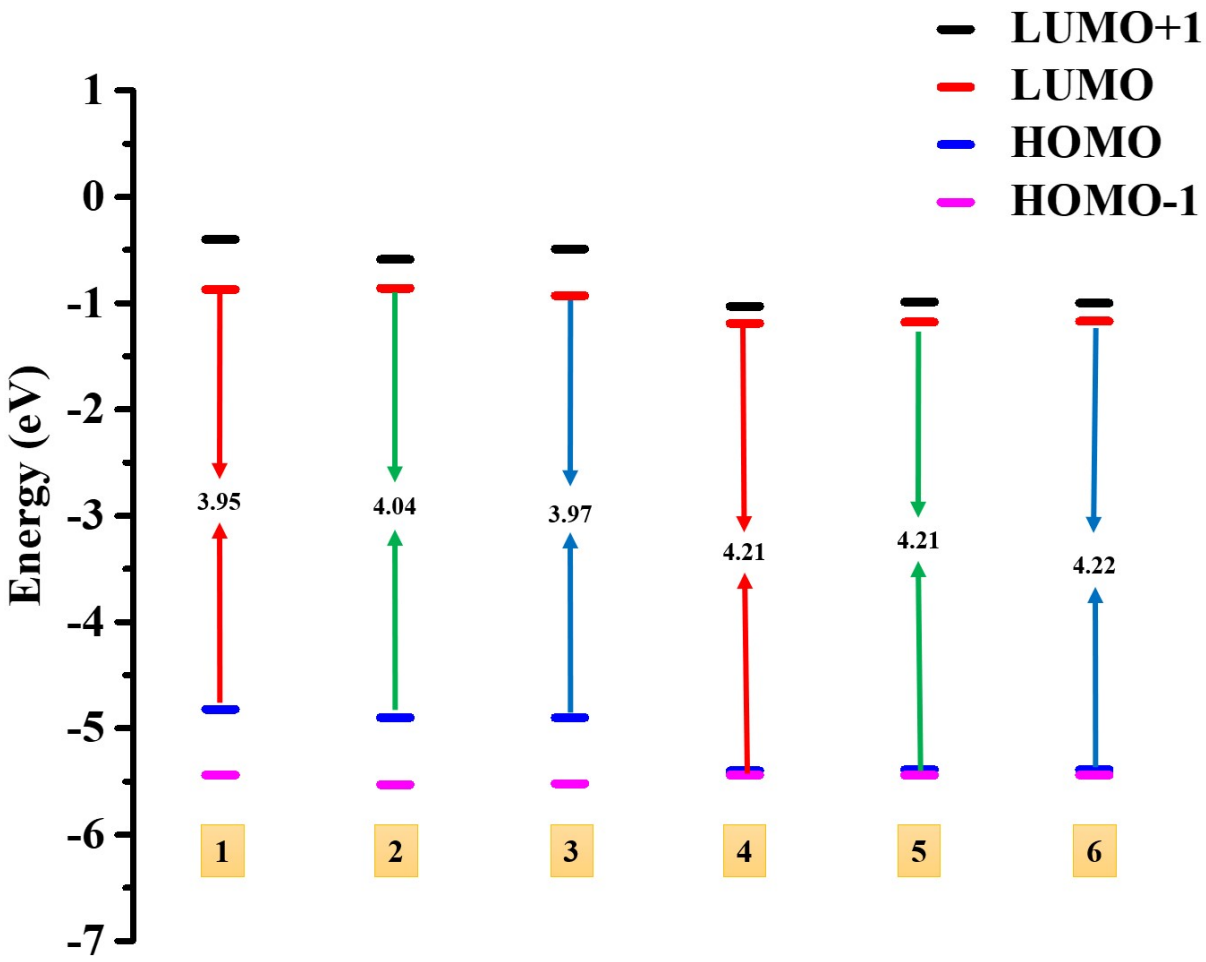

Fig. S2. Energy levels diagram of the frontier orbitals of **1–6** estimated by DFT calculations.

Table S1: Energy levels and their differences in a molecular system.

Compounds	HOMO-1	HOMO	LUMO	LUMO+1	$H-H_{-1}$	L-H	$L_{+1}-L$
1	-5.44	-4.82	-0.87	-0.40	0.62	3.95	0.47
2	-5.53	-4.90	-0.86	-0.59	0.63	4.04	0.27
3	-5.52	-4.90	-0.93	-0.49	0.62	3.97	0.44
4	-5.44	-5.40	-1.19	-1.03	0.04	4.21	0.16
5	-5.44	-5.39	-1.18	-0.99	0.05	4.21	0.19
6	-5.44	-5.39	-1.17	-1.00	0.05	4.22	0.17

TD-DFT Calculations:

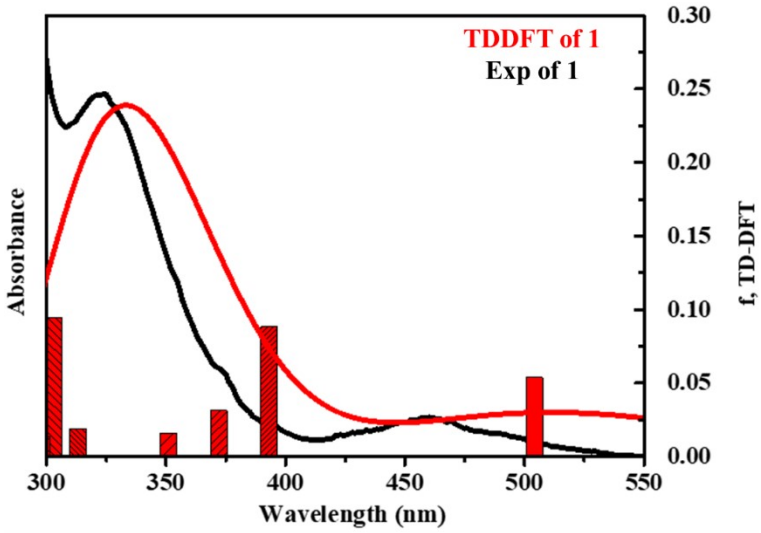

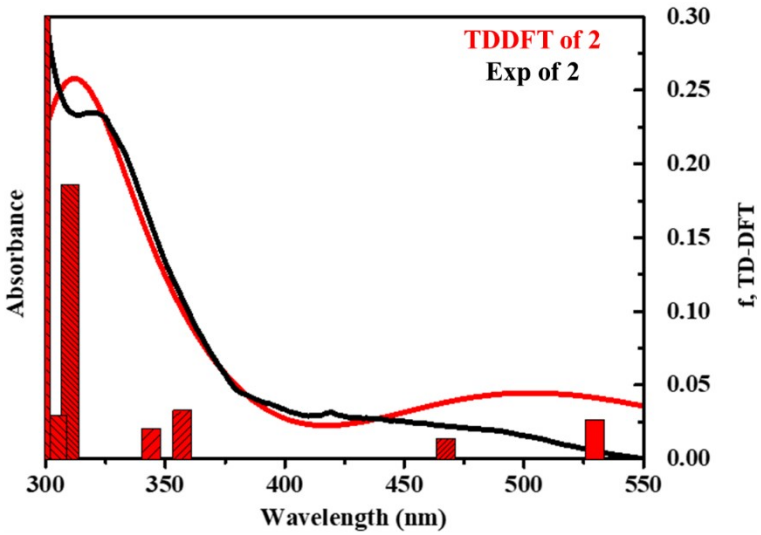

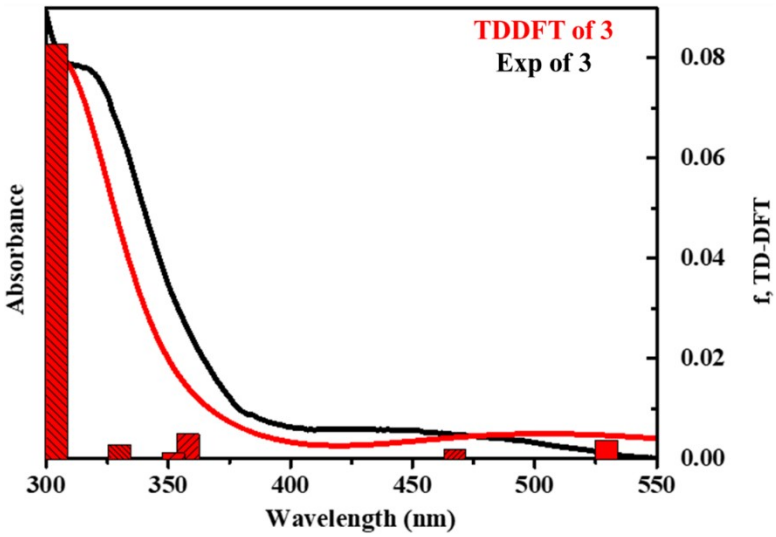

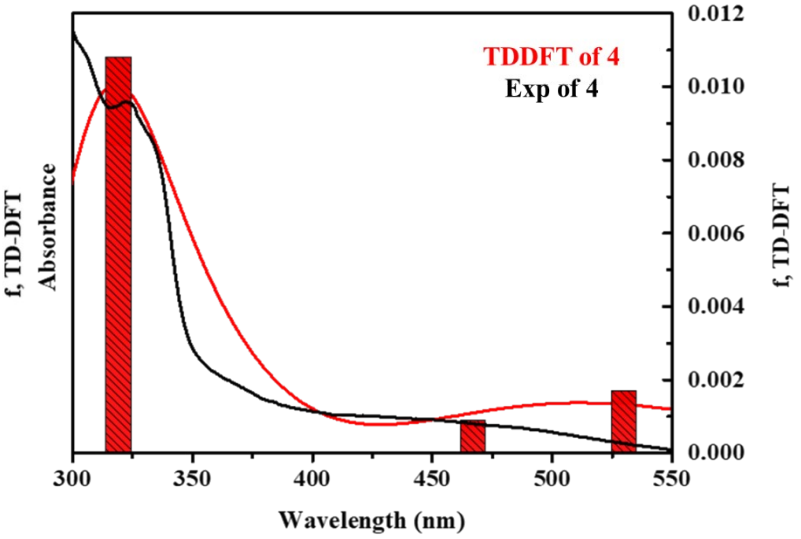

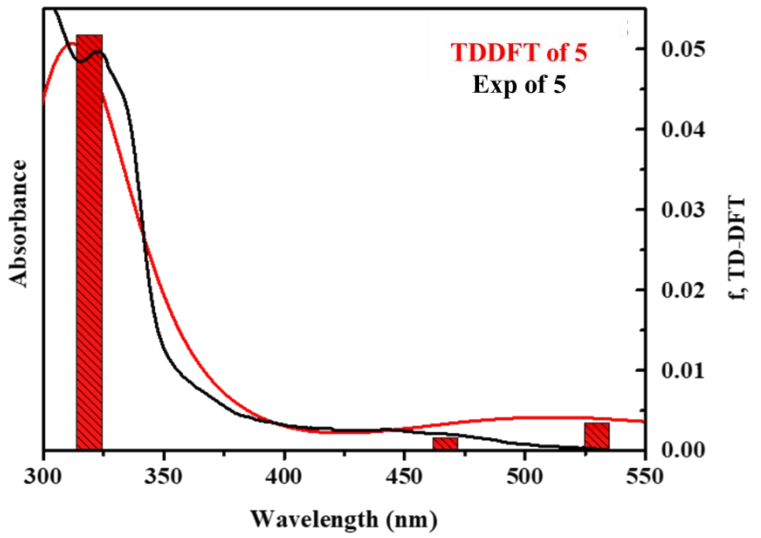

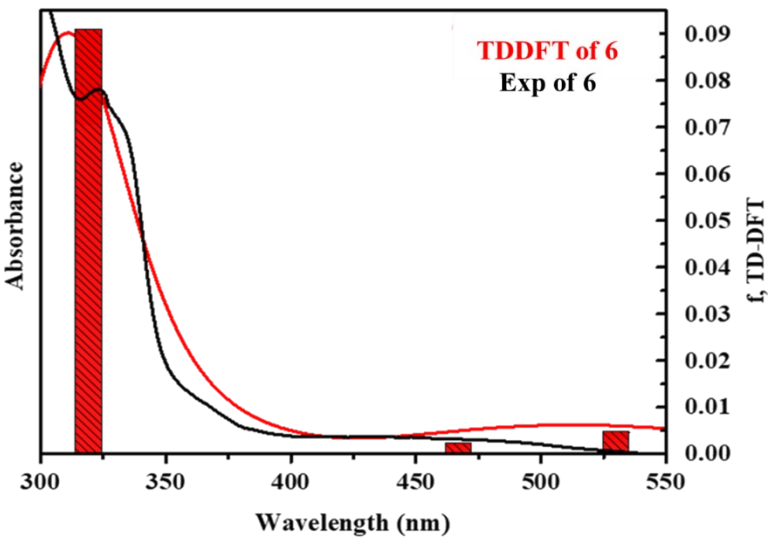

Fig. S3. Experimental (black) and TD-DFT-predicted (red) UV-Vis absorption spectra of **1**–**6** in DCM.

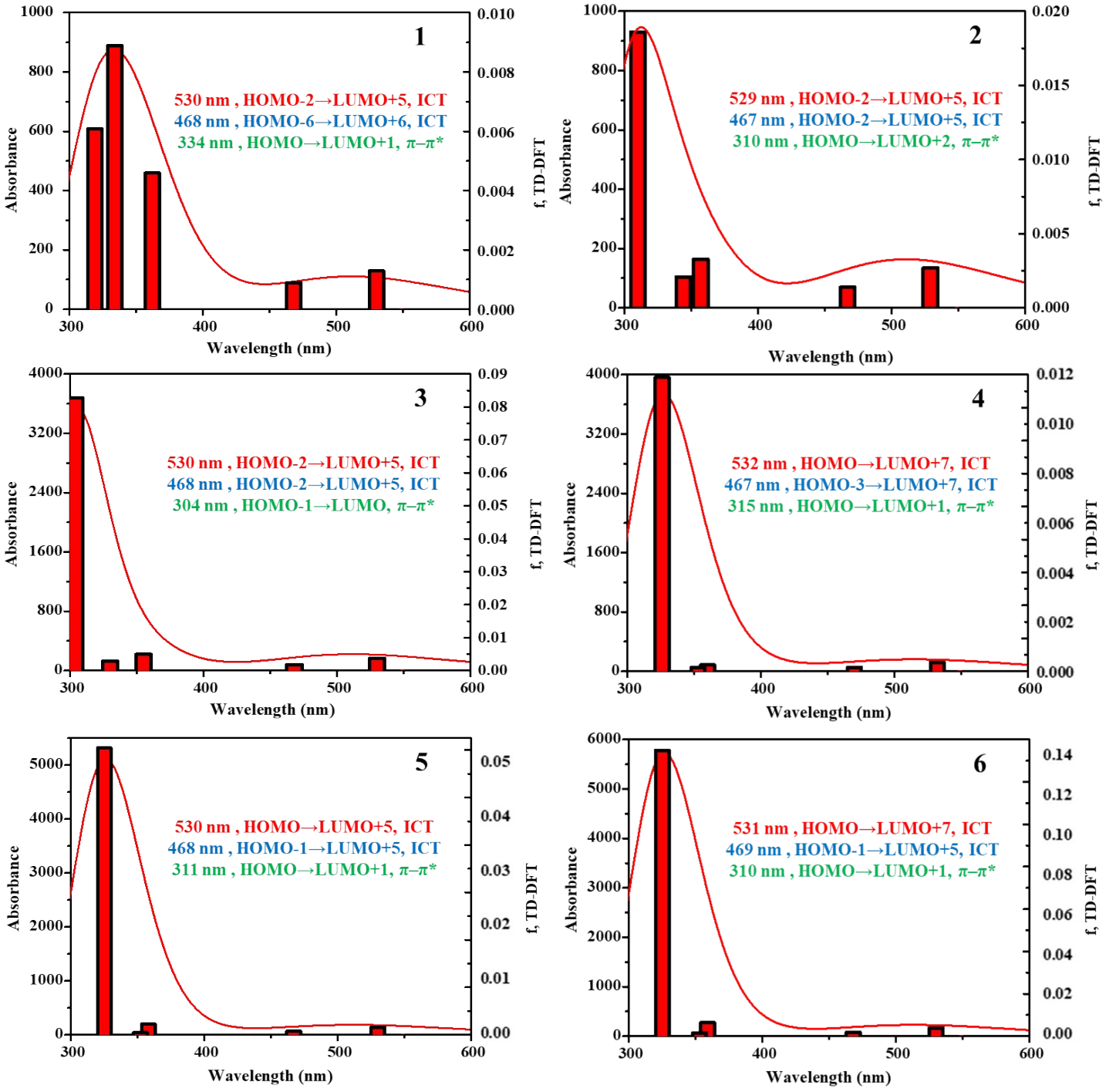

Fig. S4. TDDFT-predicted UV-vis absorption spectra along with the wavelengths, transitions, and corresponding assignments of **1–6** in DCM.

Theoretical Calculations on phenothiazine sulfoxide derivatives 7–9 (model compounds):

The computational analysis of the three-model phenothiazine sulfoxide[86–87] derivatives, **7–9**, was performed (Chart S2). The highest occupied molecular orbitals (HOMOs), lowest unoccupied molecular orbitals (LUMOs), and optimized geometries of **7–9** are presented in Fig. S5. Analysis of the frontier molecular orbitals (FMOs) for **7–9** indicates that the HOMO is predominantly localized on the ferrocene unit, with partial extension toward the phenylene spacer. In contrast, the LUMO is primarily localized on the phenylene spacer and extends across the entire molecule. Additionally, LUMO+1 is largely concentrated on the phenothiazine sulfoxide unit, extending into portions of the phenylene spacer, while HOMO-1 remains primarily localized on the ferrocene unit (Fig. S6). The theoretically calculated HOMOs for **7–9** are -5.36 eV, -5.36 eV, and -5.37 eV, respectively, while the calculated LUMOs are -0.98 eV, -0.90 eV, and -0.94 eV, respectively. These HOMO and LUMO values yield energy gaps of 4.38, 4.47, and 4.43 eV, respectively (Fig. S7 and Table S2). The energy gaps of the phenothiazine sulfoxide derivatives (**7–9**) are slightly larger than those of the phenothiazine sulfone derivatives (**4–6**).

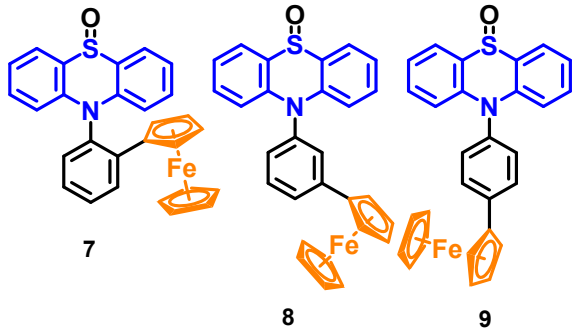

Chart S2. Molecular structures of ferrocenyl functionalized phenothiazine sulfoxide derivatives **7–9** (model compounds).

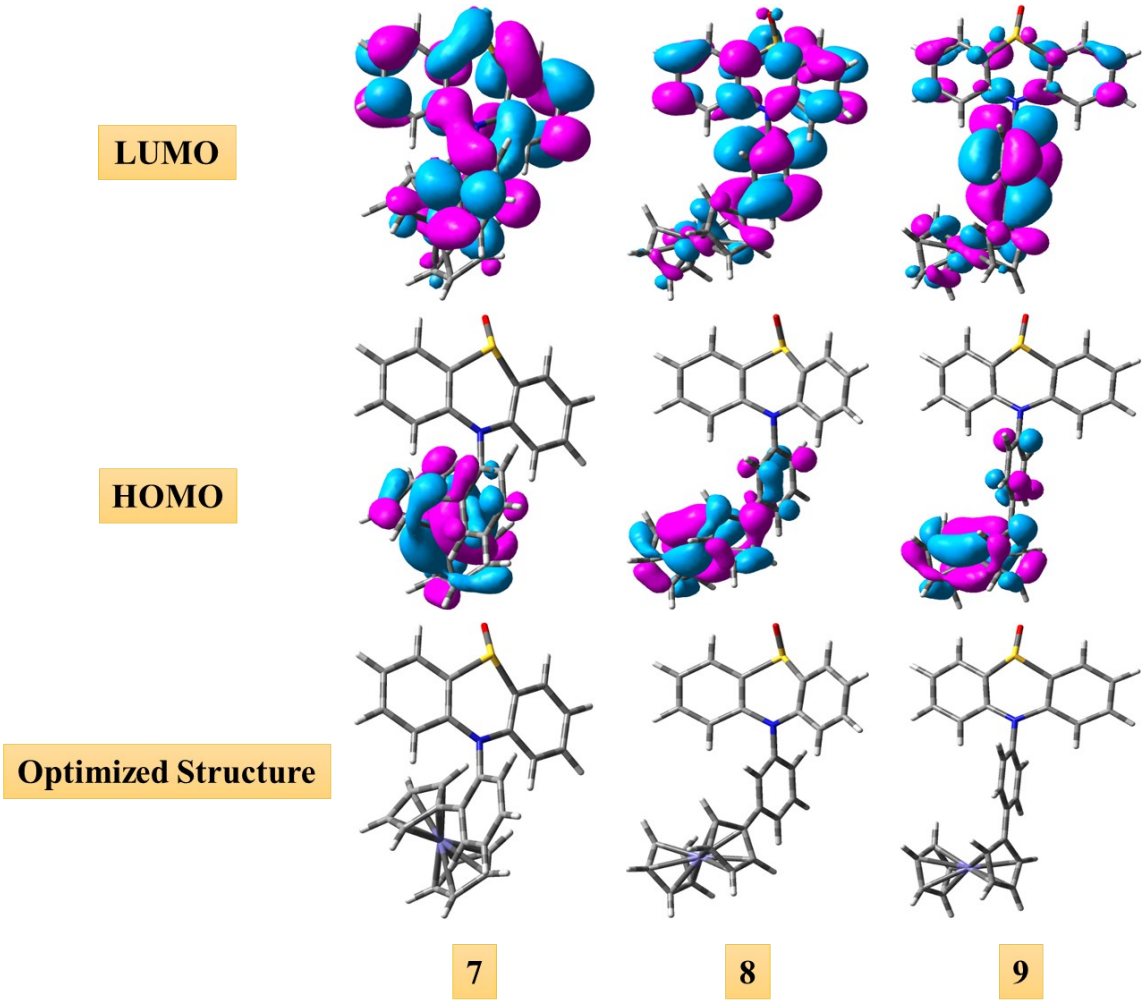

Fig. S5. Frontier HOMO and LUMO orbitals and optimized ground-state geometry of phenothiazine sulfoxide derivatives **7–9** obtained by DFT calculations.

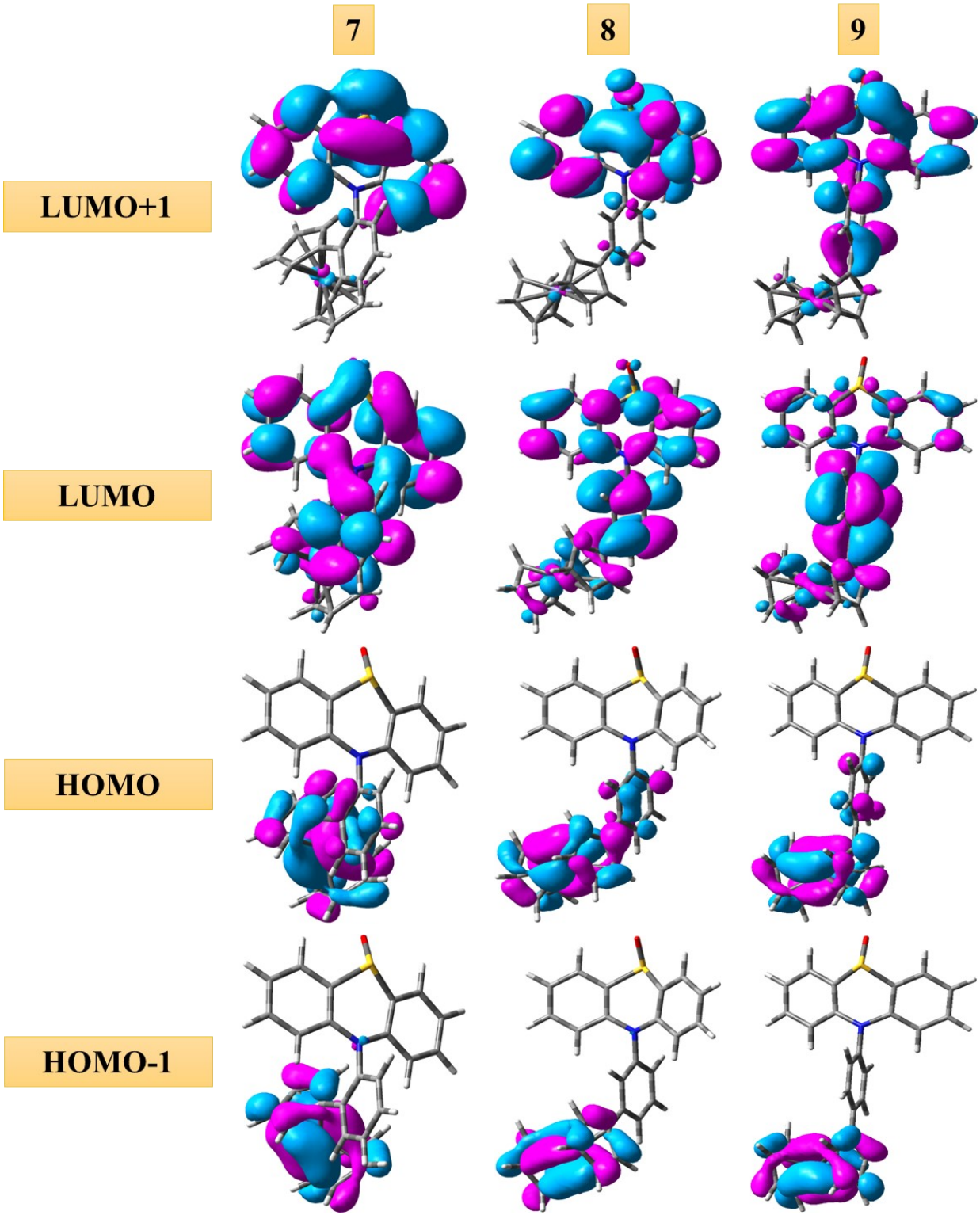

Fig. S6. The molecular orbitals of **7–9** estimated from DFT calculation.

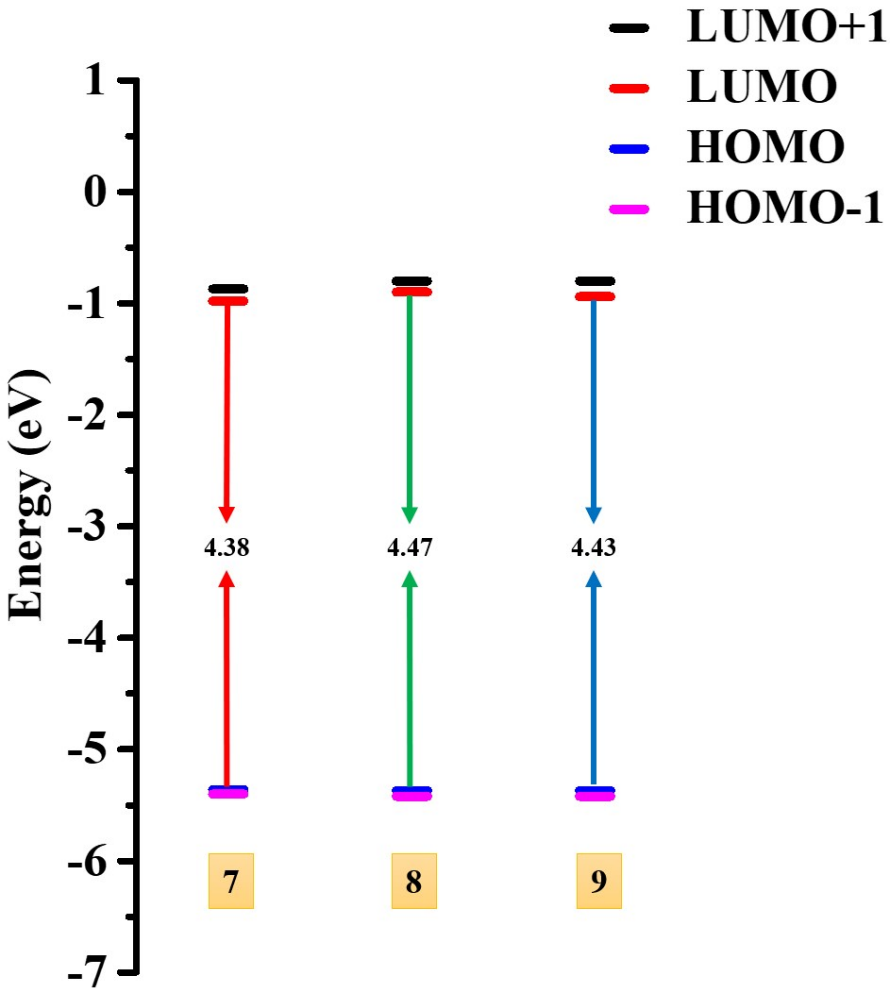

Fig. S7. Energy levels diagram of the frontier orbitals of **7–9** estimated by DFT calculations.

Table S2: Energy levels and their differences in a molecular system.

Compounds	HOMO-1	HOMO	LUMO	LUMO+1	$H-H_{-1}$	L-H	$L_{+1}-L$
7	-5.40	-5.36	-0.98	-0.87	0.04	4.38	0.11
8	-5.42	-5.37	-0.90	-0.80	0.05	4.47	0.10
9	-5.42	-5.37	-0.94	-0.80	0.05	4.43	0.14

Fluorescence Spectra:

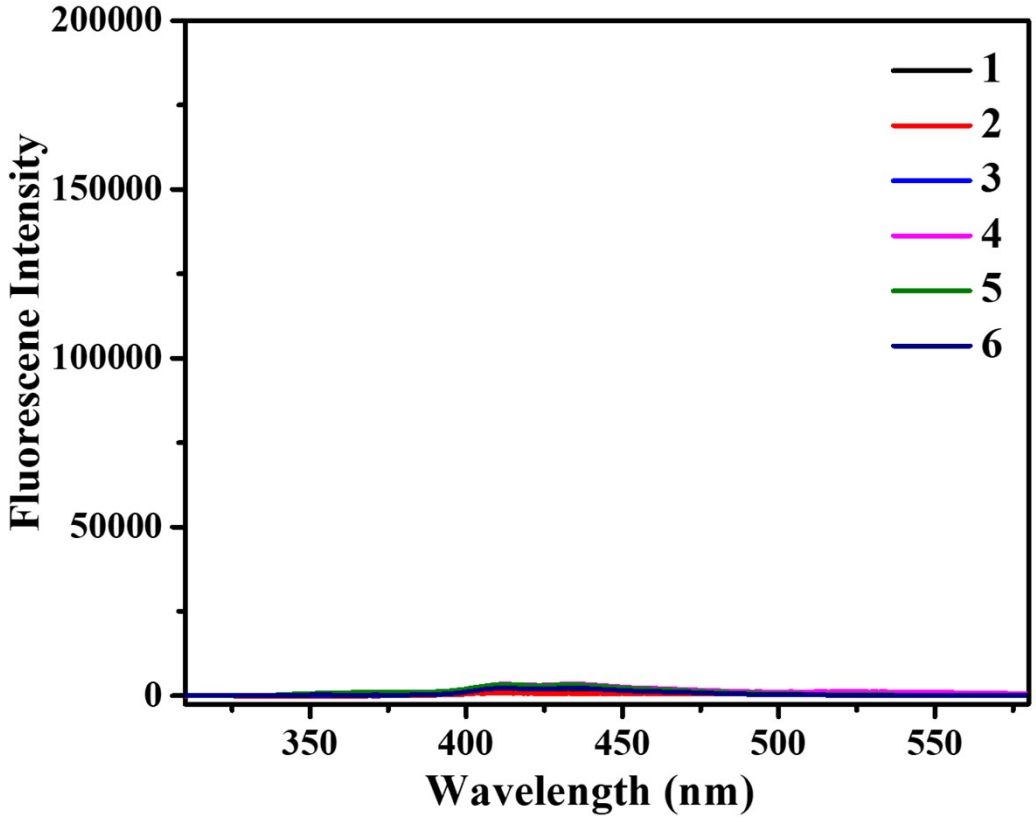

Fig. S8. Emission spectra of **1–6** in DCM.

Differential Pulse Voltammetry:

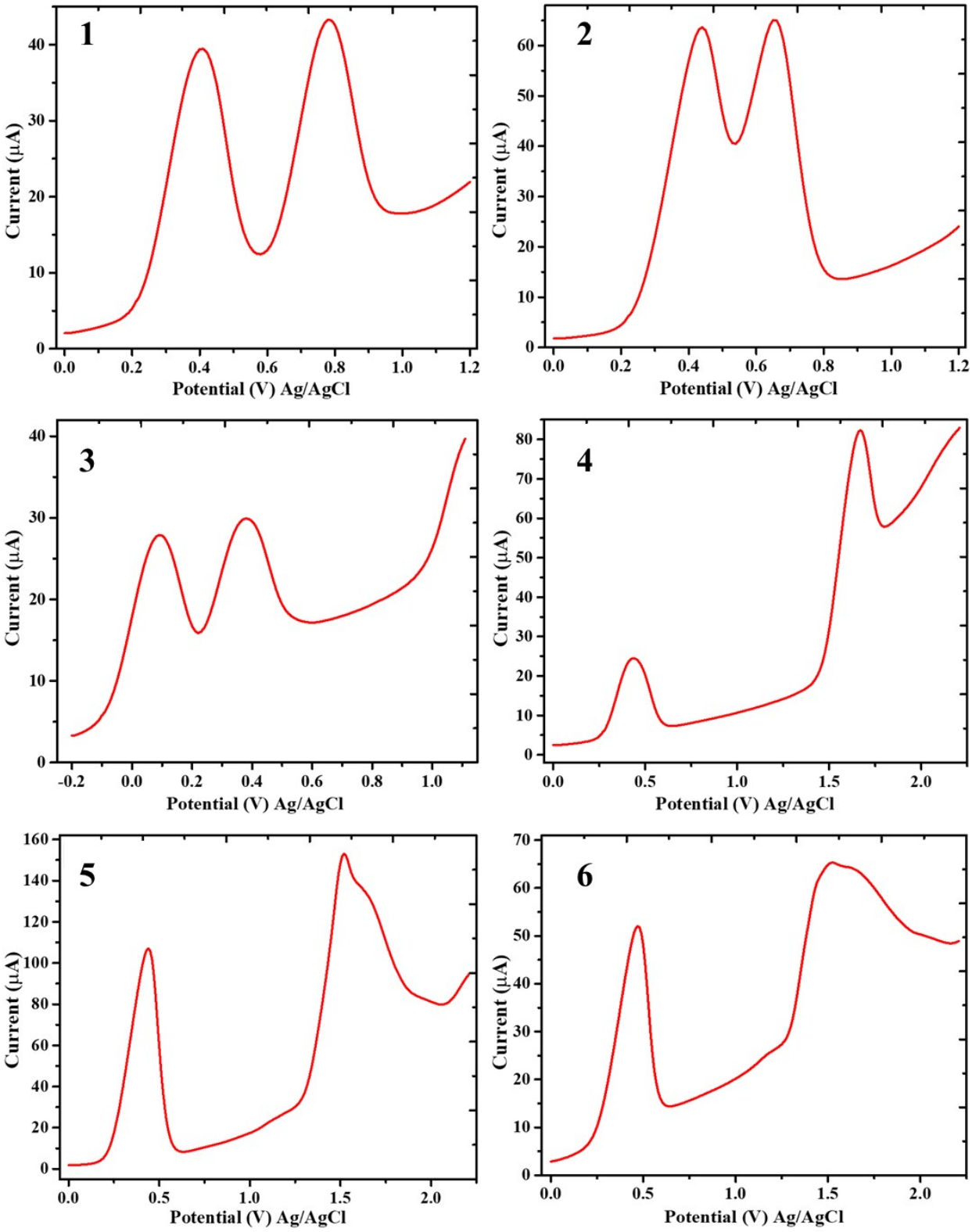

Fig. S9. Differential pulse voltammograms of **1–6** in dry dichloromethane using tetrabutylammonium hexafluorophosphate ($TBAPF_6$) as a supporting electrolyte, Pt wire as the counter electrode, glassy carbon as the working electrode, and an Ag/AgCl as the reference electrode at room temperature. The potential of ferrocene under the same conditions was determined to be 0.41 V (in DPV analysis).

Spectroelectrochemical Data:

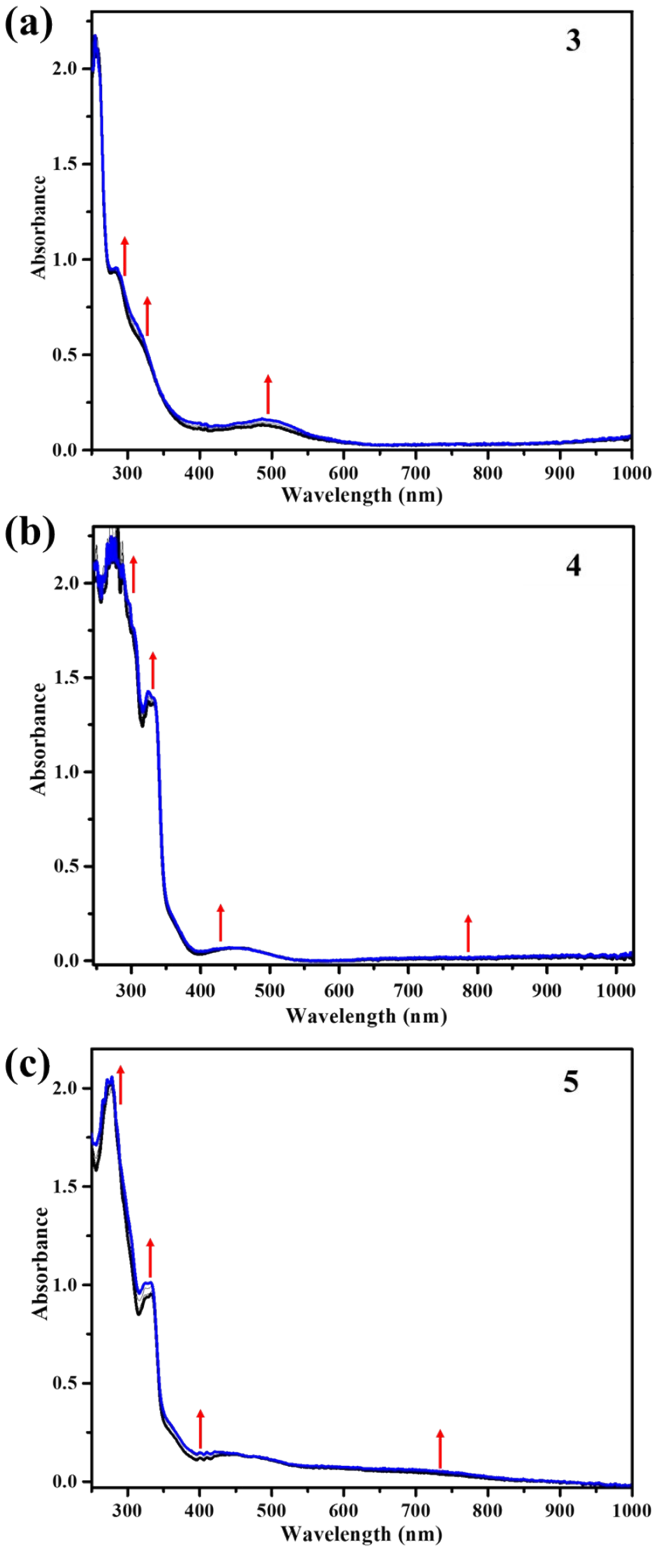

Fig. S10. Spectroelectrochemical changes observed for **3**–**5** at first (lower) oxidation cycle.

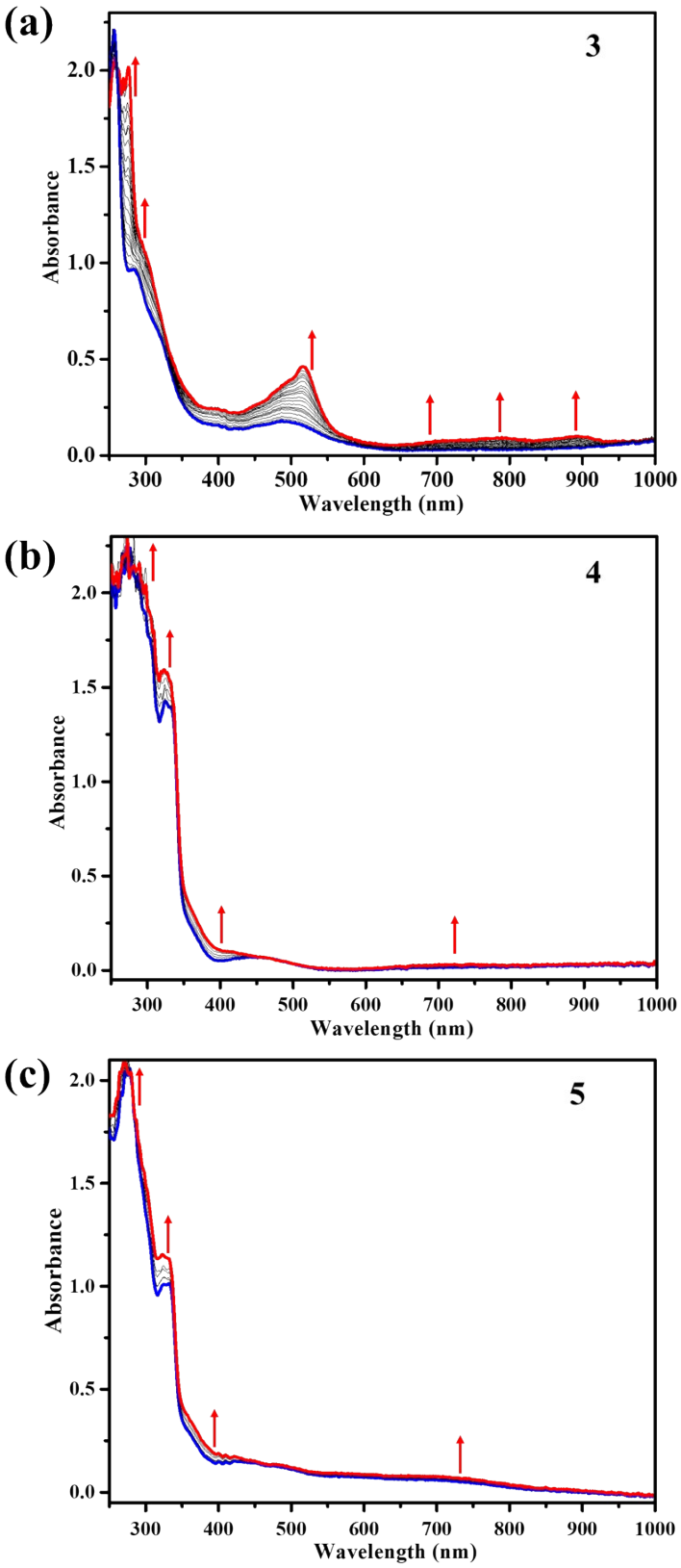

Fig. S11. Spectroelectrochemical changes observed for **3**–**5** at second (higher) oxidation cycle.

Theoretical Calculations for 1–6 radical cations:

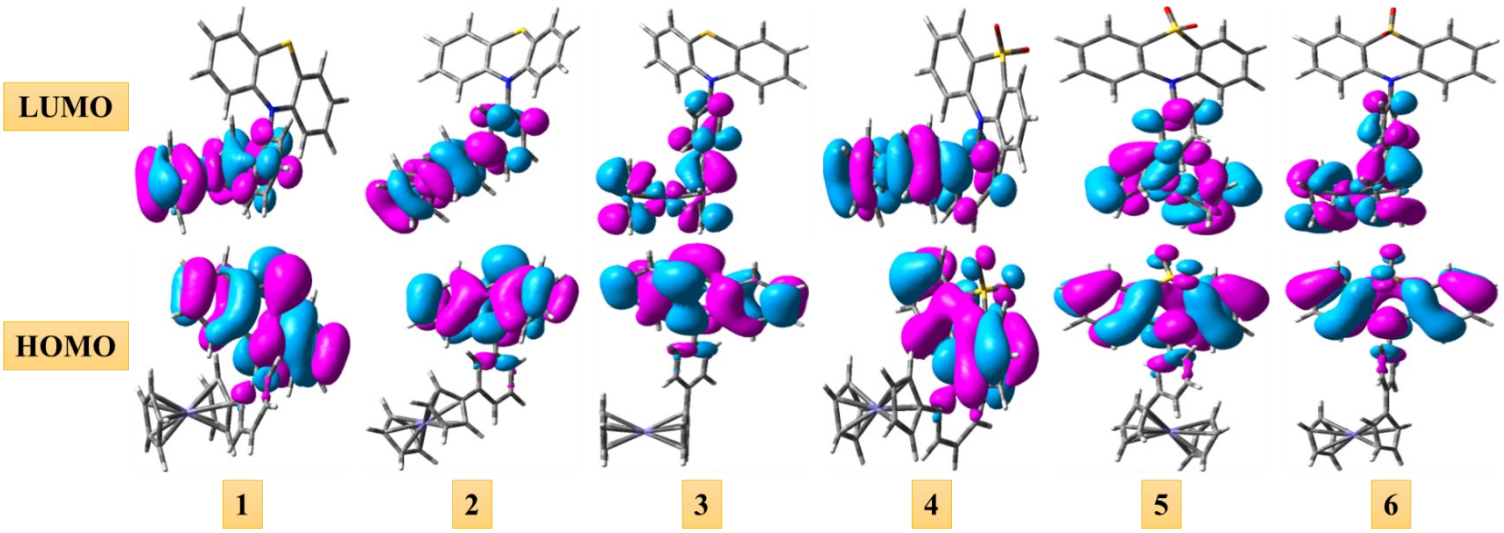

Fig. S12. Frontier HOMO and LUMO orbitals and optimized ground-state geometry of **1–6** radical cations obtained by DFT calculations.

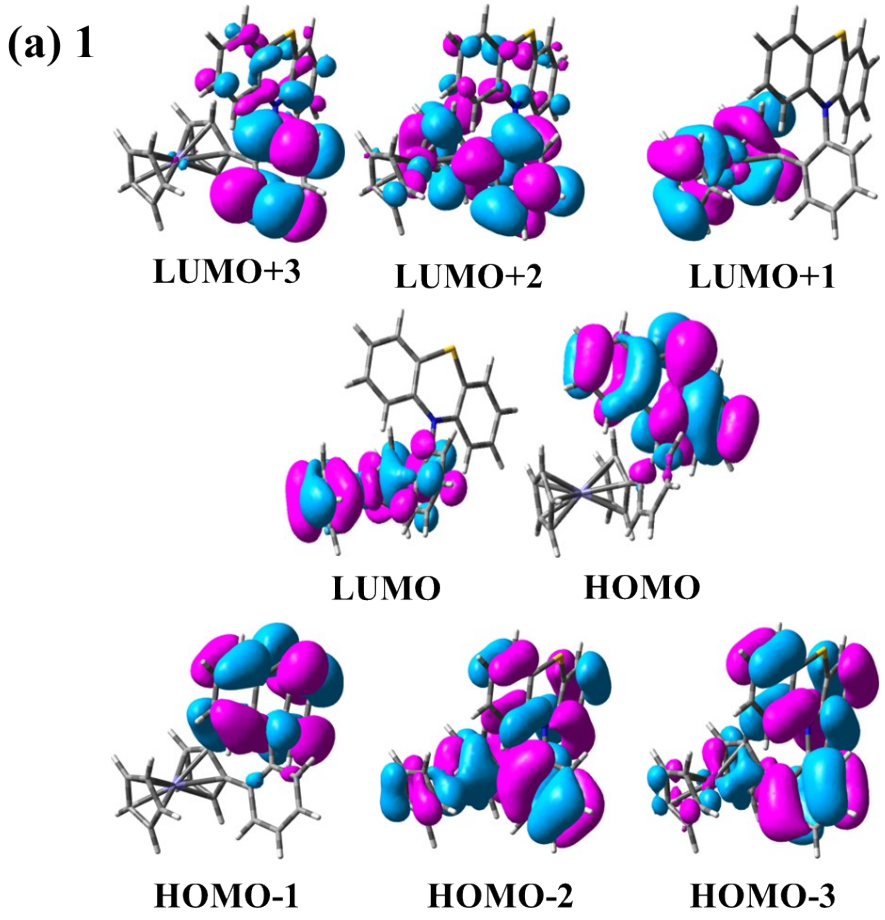

(b) 2

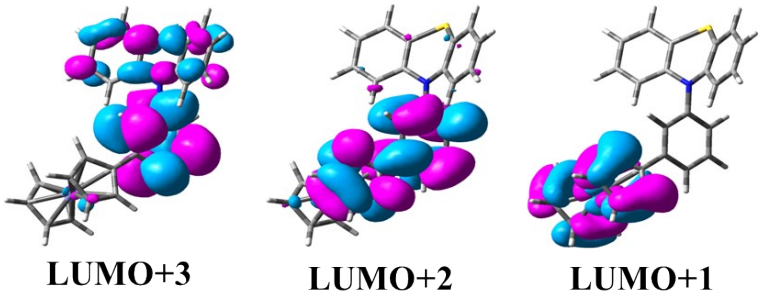

LUMO+3 LUMO+2 LUMO+1

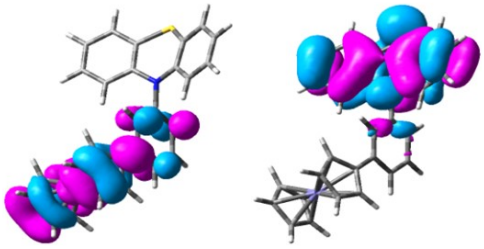

LUMO HOMO

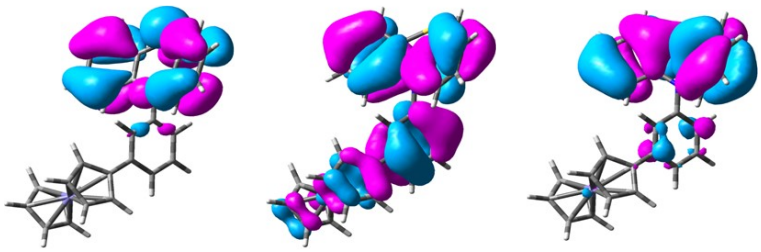

HOMO-1 HOMO-2 HOMO-3

(c) 3

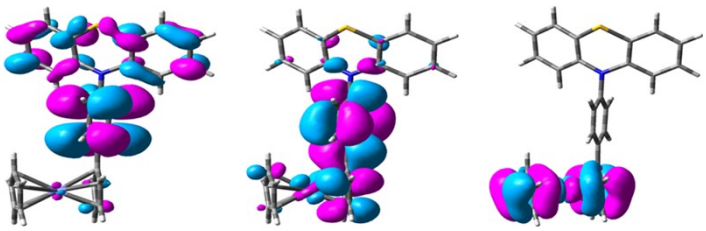

LUMO+3 LUMO+2 LUMO+1

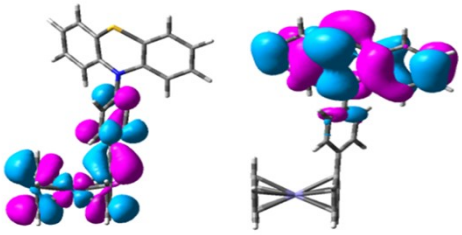

LUMO HOMO

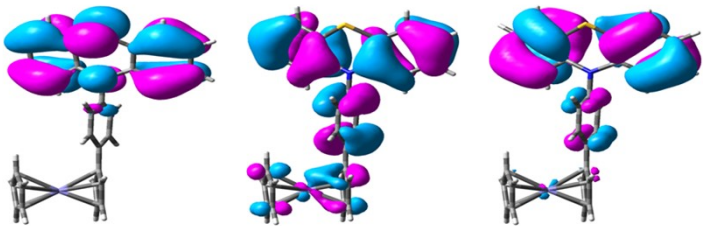

HOMO-1 HOMO-2 HOMO-3

(d) 4

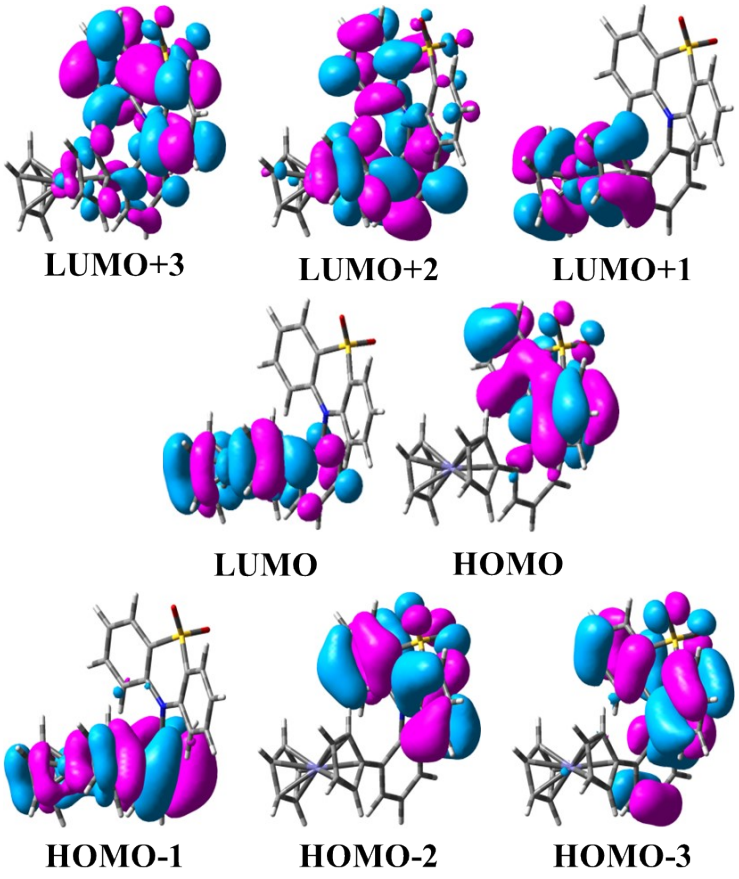
LUMO+3
LUMO+2
LUMO+1
LUMO
HOMO
HOMO-1
HOMO-2
HOMO-3

(e) 5

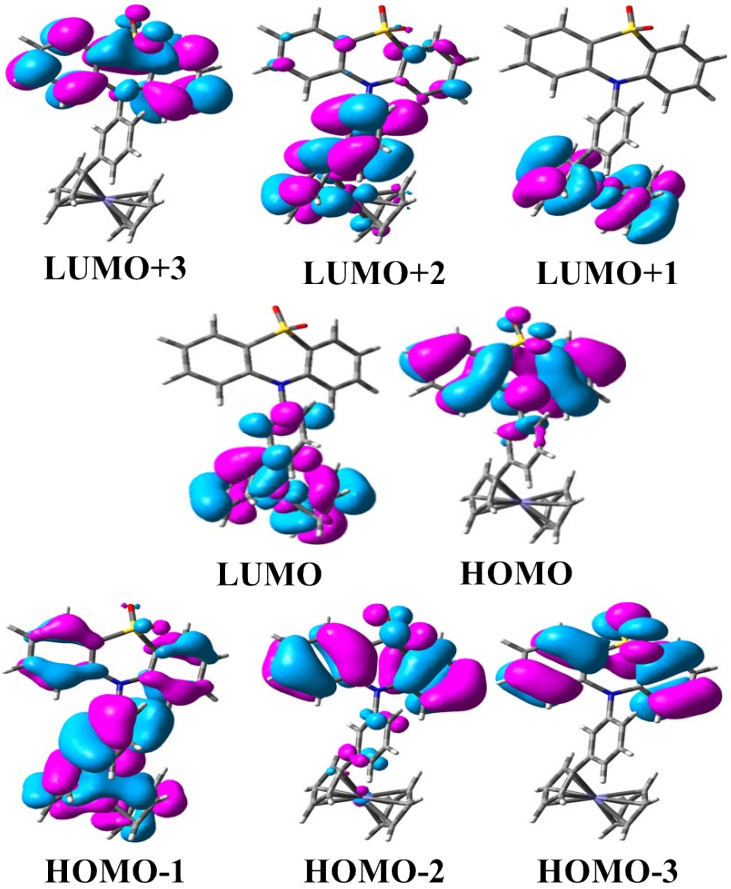
LUMO+3
LUMO+2
LUMO+1
LUMO
HOMO
HOMO-1
HOMO-2
HOMO-3

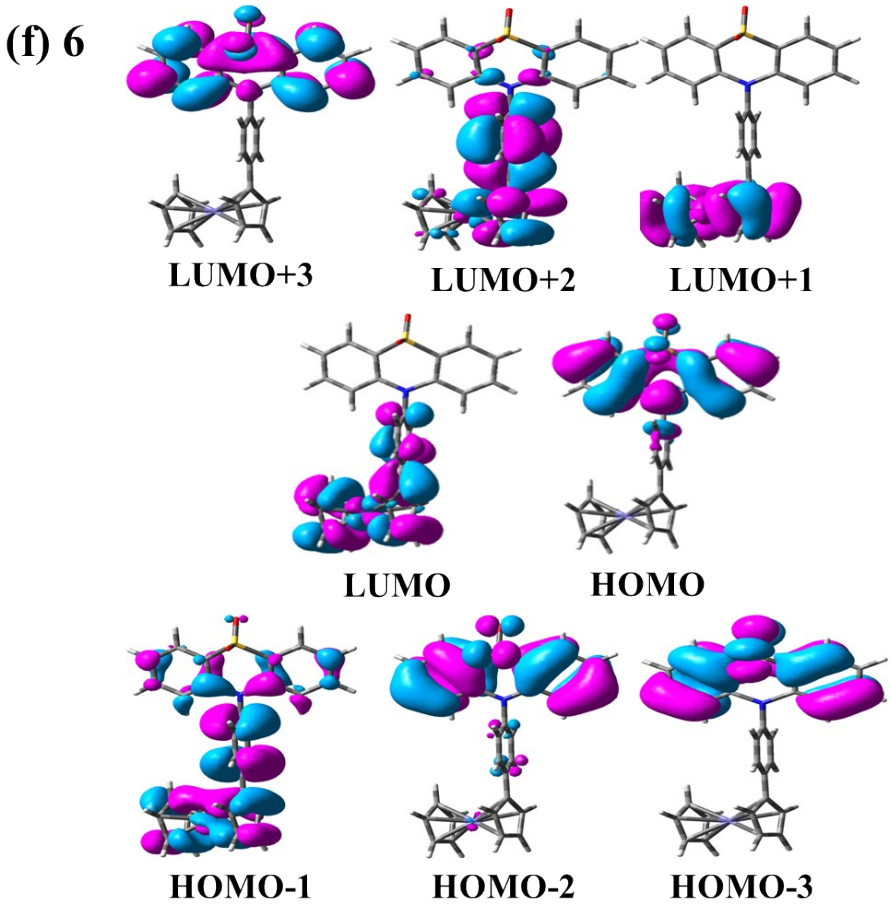

Fig. S13. The molecular orbitals of **1–6** radical cations estimated from DFT calculation.

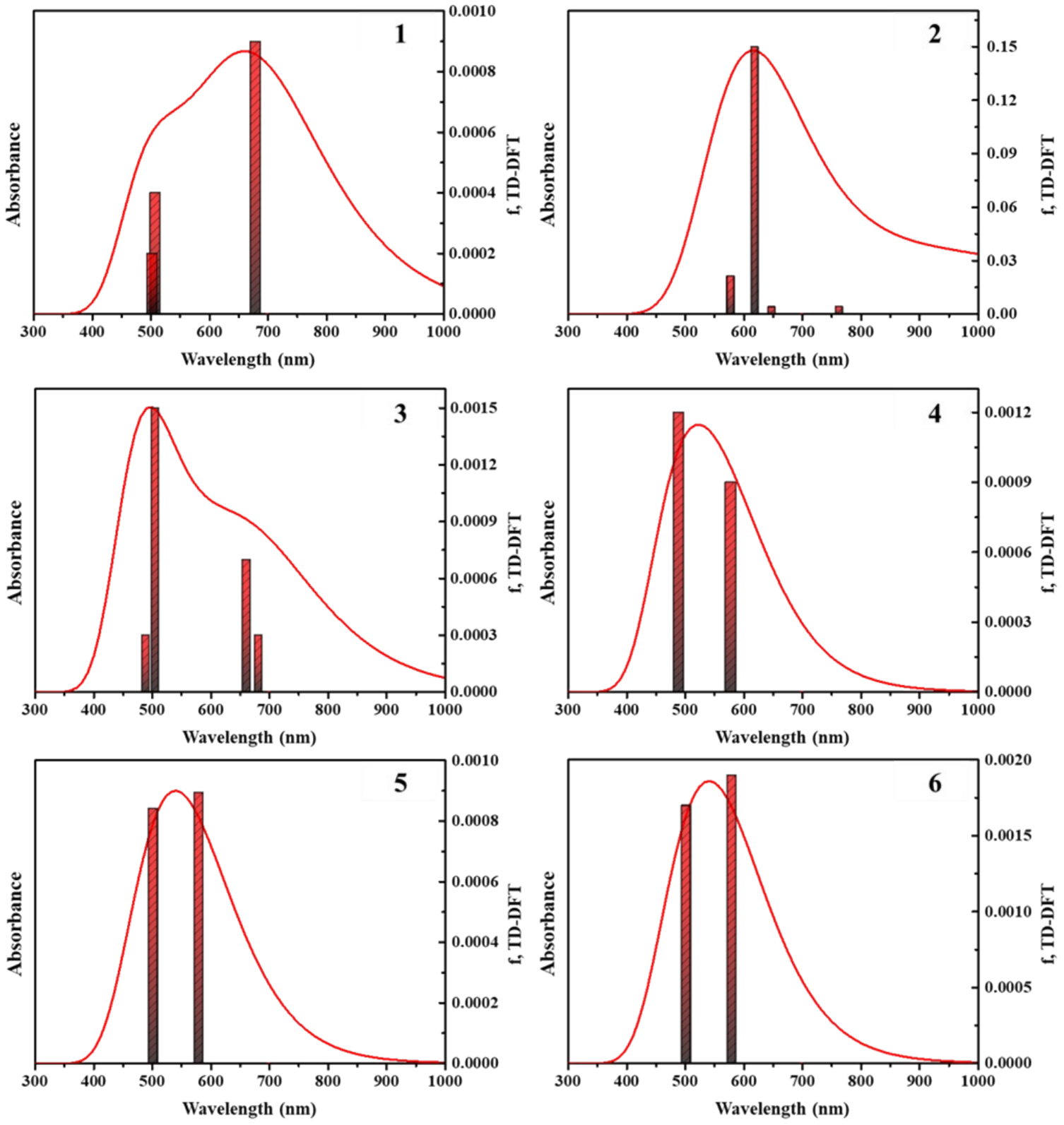

Fig. S14. TDDFT-predicted UV-vis absorption spectra of **1–6** radical cations in DCM.

Table S3: Calculated electronic transitions for **1–6** radical cations in the dichloromethane.

Compounds	Wavelengths	Composition	Molecular Contribution	f^a	Assignment
1	677	HOMO-9→LUMO+1	0.21	0.0009	ICT
	507	HOMO-8→LUMO+1	0.47	0.0004	ICT
	503	HOMO-9→LUMO	0.30	0.0002	π–π*
2	762	HOMO→LUMO	0.83	0.0043	ICT
	618	HOMO-8→LUMO	0.72	0.1499	ICT
	577	HOMO-2→LUMO	0.69	0.0212	π–π*
3	681	HOMO-7→LUMO+1	0.44	0.0003	ICT
	660	HOMO-7→LUMO+1	0.54	0.0007	ICT
	504	HOMO-2→LUMO	0.40	0.0003	π–π*
4	577	HOMO-8→LUMO	0.48	0.0009	ICT
	488	HOMO-1→LUMO	0.66	0.0012	π–π*
5	579	HOMO-6→LUMO+2	0.11	0.0017	ICT
	501	HOMO-1→LUMO	0.70	0.0016	π–π*
6	577	HOMO-7→LUMO	0.55	0.0019	ICT
	499	HOMO-1→LUMO	0.69	0.0017	π–π*

Differential Scanning Calorimetry:

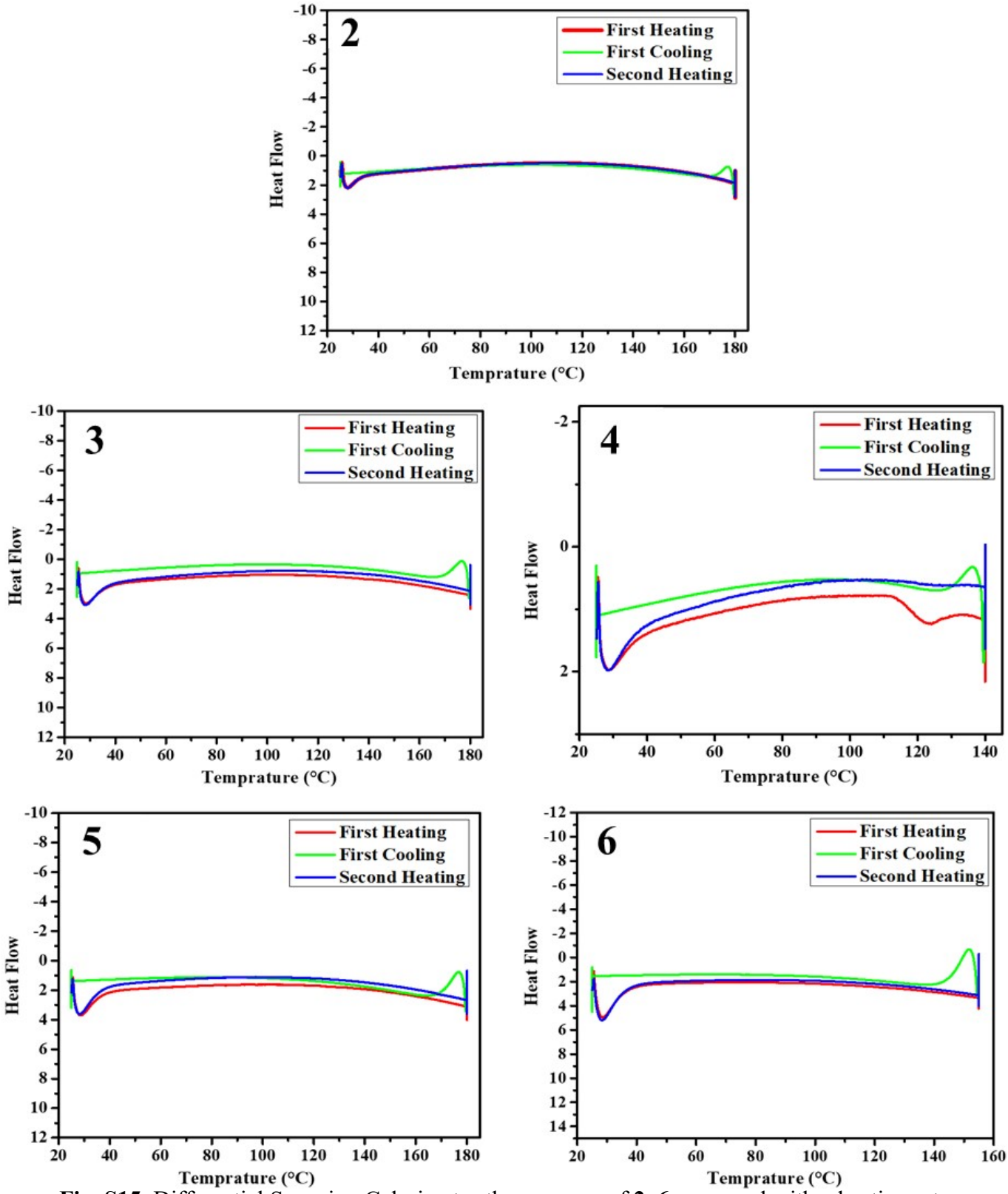

Fig. S15. Differential Scanning Calorimetry thermogram of **2–6** measured with a heating rate of 10 °C min-1 under nitrogen atmosphere.

Single Crystal X-ray Diffraction Studies:

Single crystal X-ray structural studies of **1–6** were performed on a CCD Agilent Technologies (Oxford Diffraction) SUPER NOVA diffractometer. Data were collected at 293(2) K using graphite-monochromated Mo Kα radiation (λ_α = 0.71073 Å). Unit cell determination, data collection and reduction, and empirical absorption correction were performed using the CrysAlisPro program. The data were collected by the standard 'phi-omega scan techniques, and were scaled and reduced using CrysAlisPro RED software. The Olex 2–1.5 program[2] was used as the graphical interface. The structures were solved by direct methods using SHELXT,[3] which revealed the positions of all not disordered non-hydrogen atoms. The structure model was refined using full matrix least squares minimization on F^2 using ShelXL[4] within Olex2 for a graphical interface. The positions of all the atoms were obtained by direct methods. All non-hydrogen atoms were refined anisotropically. The remaining hydrogen atoms were placed in geometrically constrained positions, and refined with isotropic temperature factors, generally 1.2U_{eq} of their parent atoms. The crystal and refinement data are summarized in Tables S4 and S5. The CCDC numbers 2324371, 2324373, 2324376, 2324375, 2324378, and 2324372 contain the supplementary crystallographic data for **1–6** respectively. These data can be obtained free of charge *via* www.ccdc.cam.ac.uk/conts/retrieving.html (or from the Cambridge Crystallographic Data Centre, 12 union Road, Cambridge CB21 EZ, UK; Fax: (+44) 1223-336 033; or deposit@ccdc.cam.ac.uk) and and Fachinformationszentrum Karls ruhe Access Structures service.

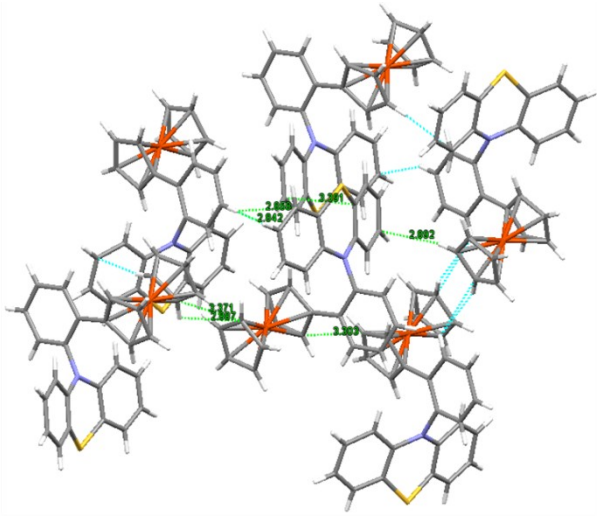

1

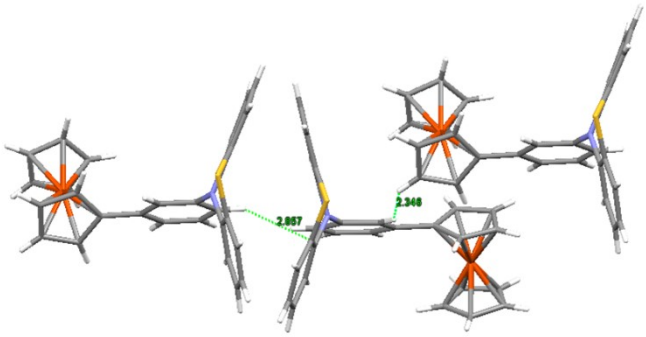

2

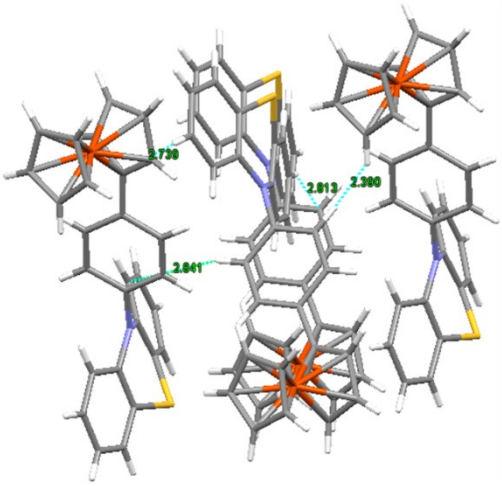

3

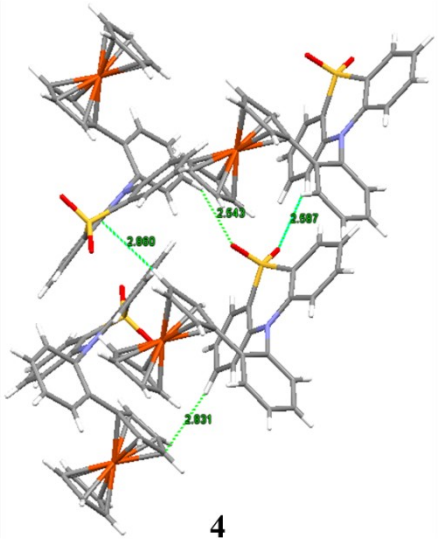

4

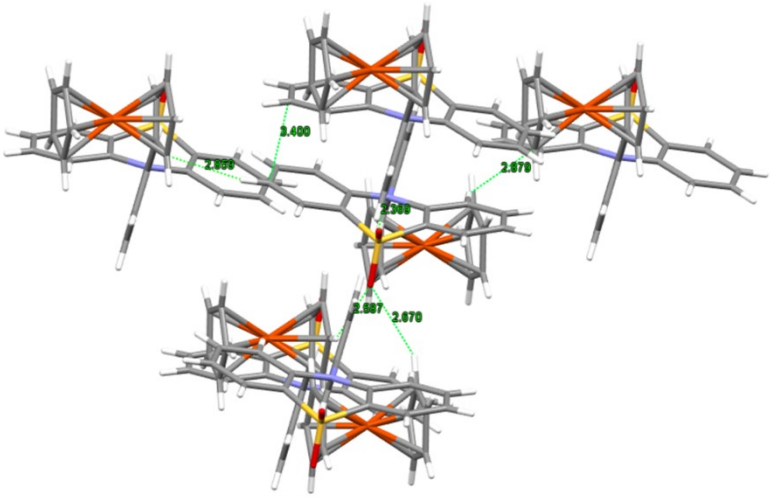

5

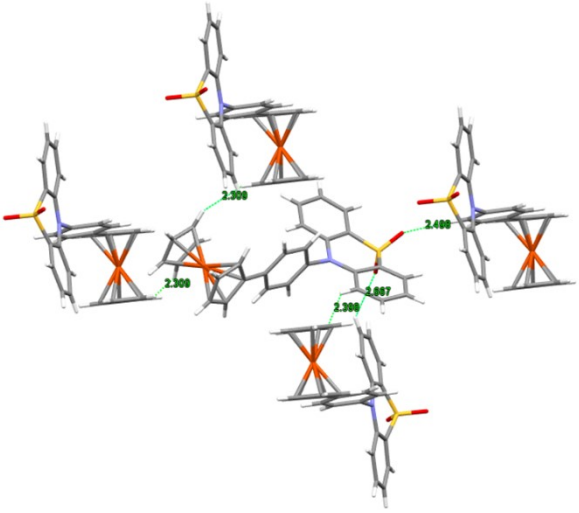

6

Fig. S16. All the different interactions between the packing diagram of the **1–6** unit.

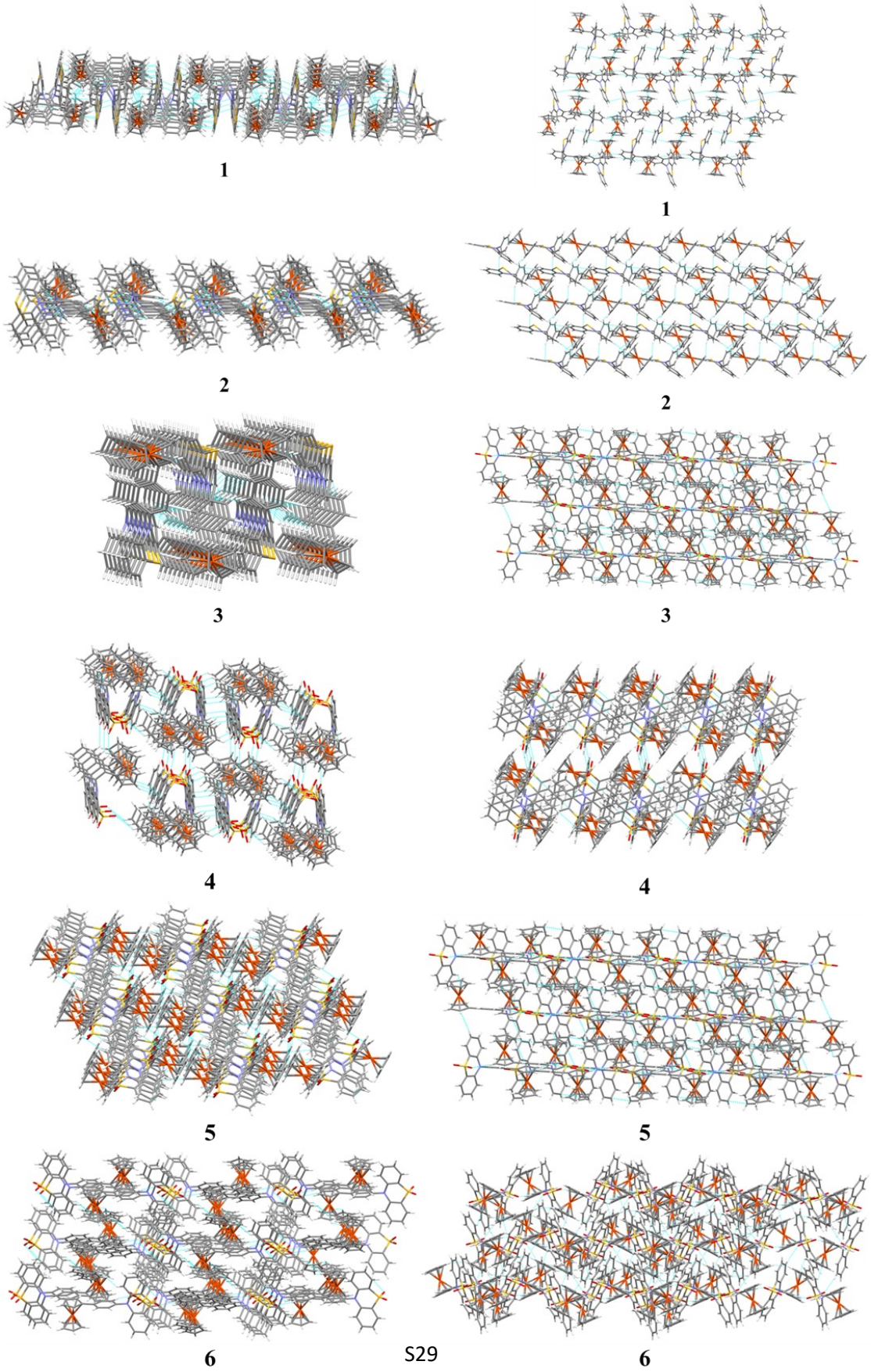

Fig. S17. Crystal packing diagrams of the **1–6**.

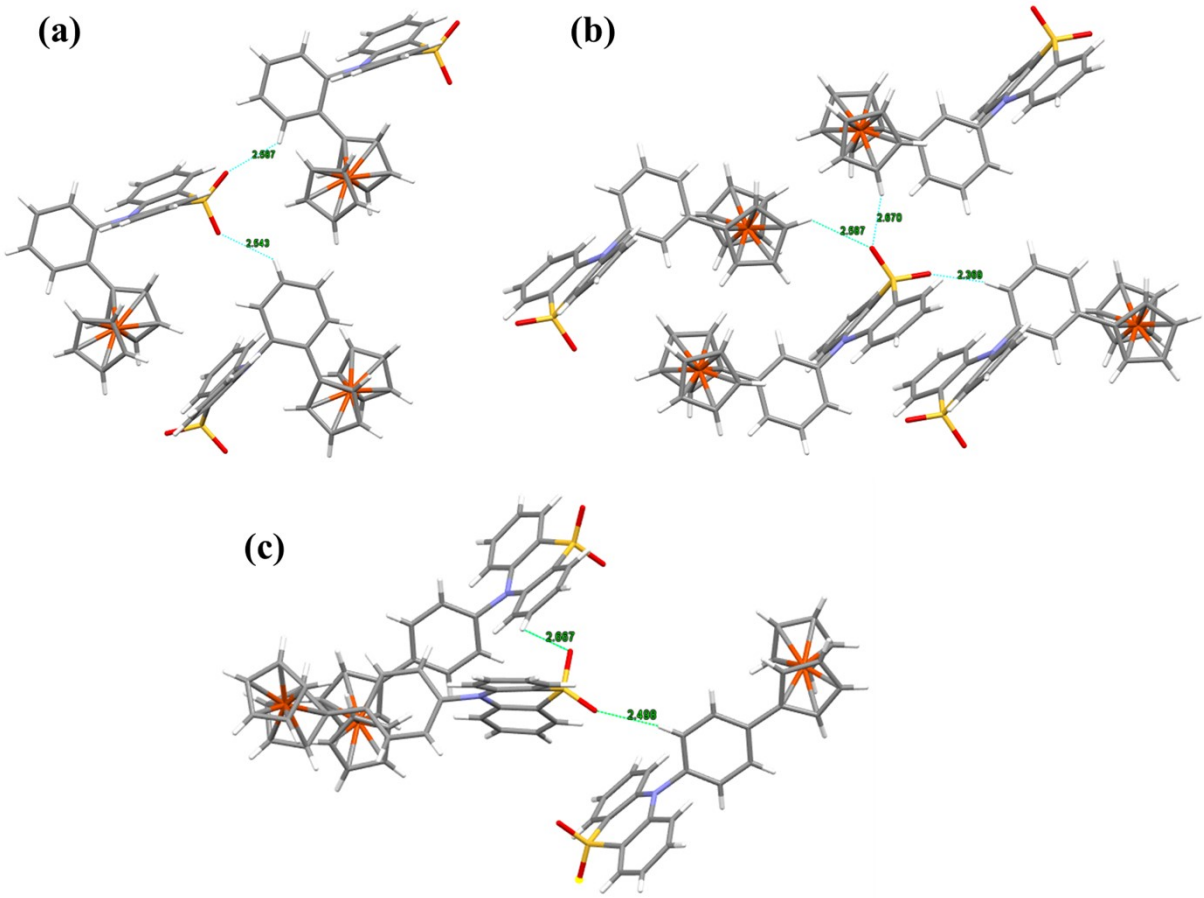

Fig. S18. All the different intermolecular hydrogen bonding interactions between the packing diagram of the (a) **4**, (b) **5**, and (c) **6**.

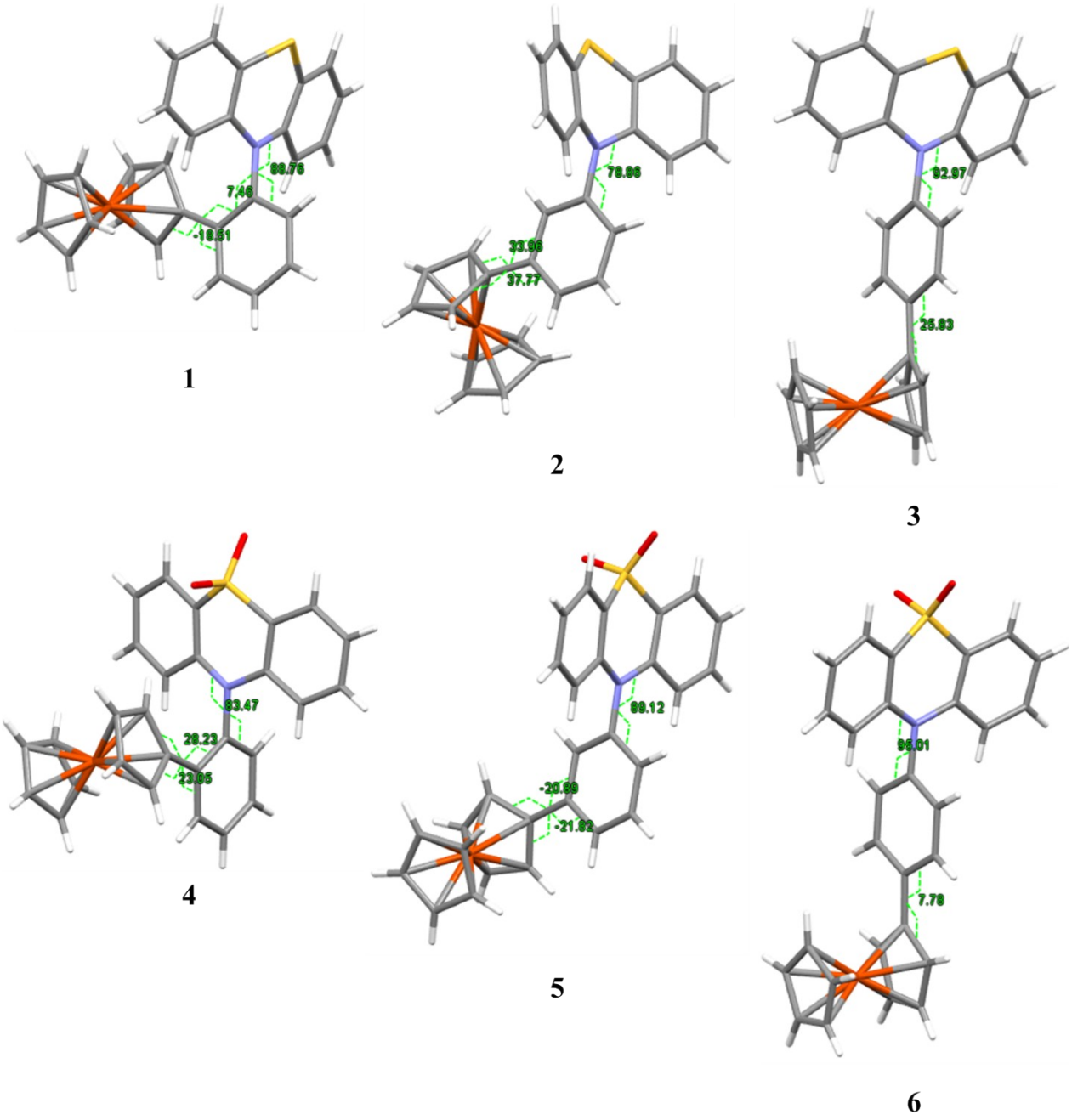

Fig. S19. Torsion angles between the key atoms of phenothiazine, phenyl, and ferrocene unit of the **1–6**.

Table S4. Crystal data and structure refinement for 1–3.

	1	2	3
Identification Code	N_1	RM-676	RM687B
Empirical Formula	$C_{28}H_{21}FeNS$	$C_{28}H_{21}FeNS$	$C_{28}H_{21}FeNS$
Formula Weight	459.37	459.37	459.37
Temperature/K	298.00	298.00	298.00
Crystal System	monoclinic	monoclinic	monoclinic
Space Group	$P2_1/n$	$P2_1$	$P2_1/n$
a/(Å)	16.3068(4)	7.67609(3)	8.7645(7)
b/(Å)	13.9523(2)	10.4925(3)	25.8133 (8)
c/(Å)	19.3646(5)	13.5049(6)	10.1975(16)
α /(deg)	90	90	90
β/(deg)	104.722(2)	102.663(4)	111.404(9)
γ/(deg)	90	90	90
Volume/ (Å)³	4261.14(17)	1061.23(7)	2148.0(3)
Z	8	2	4
Dx (Mg m⁻³)	1.432	1.438	1.420
F(000)	0.822	0.825	0.815
μ (mm⁻¹)	1904.0	476.0	952.0
Θ range for data collection(deg)	1.32x1.25x1.02	1.35 x 1.17 x 1.1	3.2 x 1.35 x 1.1
Limiting indices	Mo K*α* *(λ = 0.71073)*	Mo K*α* *(λ = 0.71073)*	Mo K*α* *(λ = 0.71073)*
Reflections collected	5.852 to 58.294	6.184 to 58.476	6.39 to 58.25
unique reflections	$-21 \le h \le 21$, $-17 \le k \le 19$, $-25 \le -1 \le 24$	$-9 \le h \le 9$, $-14 \le k \le 14$, $-13 \le 1 \le 18$	$-11 \le h \le 11$, $-34 \le k \le 34$, $-12 \le 1 \le 13$
R(int)	42219	8197	18743
Completeness to θ	10390 [R_{int} = 0.0650, R_{sigma} = 0.0695]	4388 [R_{int} = 0.1301, R_{sigma} = 0.1392]	5262 [R_{int} = 0.1276, R_{sigma} = 0.1263]
Data/restraints/parameters	10390/0/560	4388/1/280	5262/0/280
GOF on F^2	1.062	1.034	1.032
R1 and R2 [I>2σ(I)]	R_1=0.0548, wR_2 = 0.1089	R_1=0.0701, wR_2 = 0.1679	R_1=0.0716, wR_2 = 0.1473
R1 and R2 (all data)	R_1 = 0.1121, wR_2 = 0.1393	R1=0.1171, wR2 = 0.2275	R_1=0.1300, wR_2 = 0.1821
Largest diff. peak and hole(e.A⁻³)	0.34/-0.54	0.56/-1.11	0.69/-0.54

Table S5. Crystal data and structure refinement for 4–6.

	4	**5**	**6**
Identification Code	RM677	RM 686	RM 683
Empirical Formula	$C_{28}H_{21}NO_2SFe$	$C_{28}H_{21}NO_2SFe$	$C_{28}H_{21}NO_2SFe$
Formula Weight	491.37	491.37	491.37
Temperature/K	298.00	293.00	293.00
Crystal System	monoclinic	triclinic	monoclinic
Space Group	$P2_1/c$	P-1	$P2_1/c$
a/(Å)	11.0450(4)	9.58604(4)	14.5069(4)
b/(Å)	15.2700(5)	11.2456(9)	11.4203 (4)
c/(Å)	14.1055(4)	11.3589(6)	13.8306(4)
α /(deg)	90	65.762(6)	90
β/(deg)	94.779(3)	85.809(4)	104.546(3)
γ/(deg)	90	82.170(5)	90
Volume/ (Å)³	2370.72(13)	1105.94(13)	2217.73(12)
Z	4	2	4
Dx (Mg m⁻³)	1.377	1.476	1.472
F(000)	0.749	0.803	0.801
μ (mm⁻¹)	1016.0	508.0	1016.0
Θ range for data collection(deg)	1.78x1.54x1.35	0.55x0.43x0.34	0.37x 1.26 x 0.24
Limiting indices	Mo K*α (λ = 0.71073)*	Mo K*α (λ = 0.71073)*	Mo K*α (λ = 0.71073)*
Reflections collected	6.382 to 58.31	5.698 to 58.532	6.812 to 58.626
unique reflections	$-14 \le h \le 14$, $-20 \le k \le 19$, $-18 \le 1 \le 18$	$-13 \le h \le 12$, $-15 \le k \le 15$, $-15 \le -1 \le 15$	$-18 \le h \le 19$, $-15 \le k \le 15$, $18 \le 1 \le 17$
R(int)	20172	24255	27175
Completeness to θ	5737 [R_{int} = 0.0683, R_{sigma} = 0.0644]	5450 [R_{int} = 0.1686, R_{sigma} = 0.1487]	5600 [R_{int} = 0.0564, R_{sigma} = 0.0386]
Data/restraints/parameters	5737/0/298	5450/0/298	5600/0/298
GOF on F^2	1.047	0.978	1.053
R1 and R2 [I>2σ(I)]	R_1=0.0522, wR_2 = 0.1223	R_1=0.0673, wR_2 = 0.1418	R_1=0.0450, wR_2 = 0.1115
R1 and R2 (all data)	R_1 = 0.0893, wR_2 = 0.1467	R_1 = 0.1457, wR_2 = 0.1838	R1=0.0601, wR2 = 0.1226
Largest diff. peak and hole(e.A⁻³)	0.33/ -0.39	0.60/-0.59	0.40/-0.39

Comparative Analysis of Bond Lengths and Angles in Ferrocene Functionalized Phenothiazine and Phenothiazine Sulfone Derivatives:

The comparable study of the selected bond lengths of the optimized DFT structure and the single crystal structure shows a slight variation in bond lengths of ferrocene functionalized phenothiazine derivatives **1–3** (Fig. S20) and ferrocene functionalized phenothiazine sulfone derivatives **4–6** (Fig. S22). In all the phenothiazine and phenothiazine sulfone derivatives both C–N bonds of the phenothiazine ring show slight variations in the bond lengths while both C–S bonds of the phenothiazine ring are almost the same in bond length. The S–O bond lengths of the single crystal structures of the phenothiazine sulfones are slightly smaller than the theoretically estimated S–O bond lengths of phenothiazine sulfones. The C–C bond length between the ferrocene and phenylene spacer is larger for the *ortho*-substituted isomers as compared to the *meta*- and *para*- substituted isomers of both the ferrocene functionalized phenothiazine and phenothiazine sulfone derivatives **1–6**.

A comparison between the bond angles of the single crystal structure and the DFT optimized structure of ferrocene functionalized phenothiazine derivatives **1–3** are shown in Fig. S21 and it indicates that the theoretically estimated bond angles for **1–3** shows a good agreement with the bond angles calculated from the single crystal structure. The comparable study of the bond angles of ferrocene functionalized phenothiazine sulfone derivatives **4–6** of the single crystal structure and the DFT optimized structure is depicted in Fig. S23 and it also indicates a good agreement with the theoretically estimated bond angles with the bond angle of the single crystal structure of phenothiazine sulfones. The C–S–C bond angles of the single crystal structures of the phenothiazine sulfones are slightly larger than the theoretically estimated C–S–C bond angles of phenothiazine sulfones.

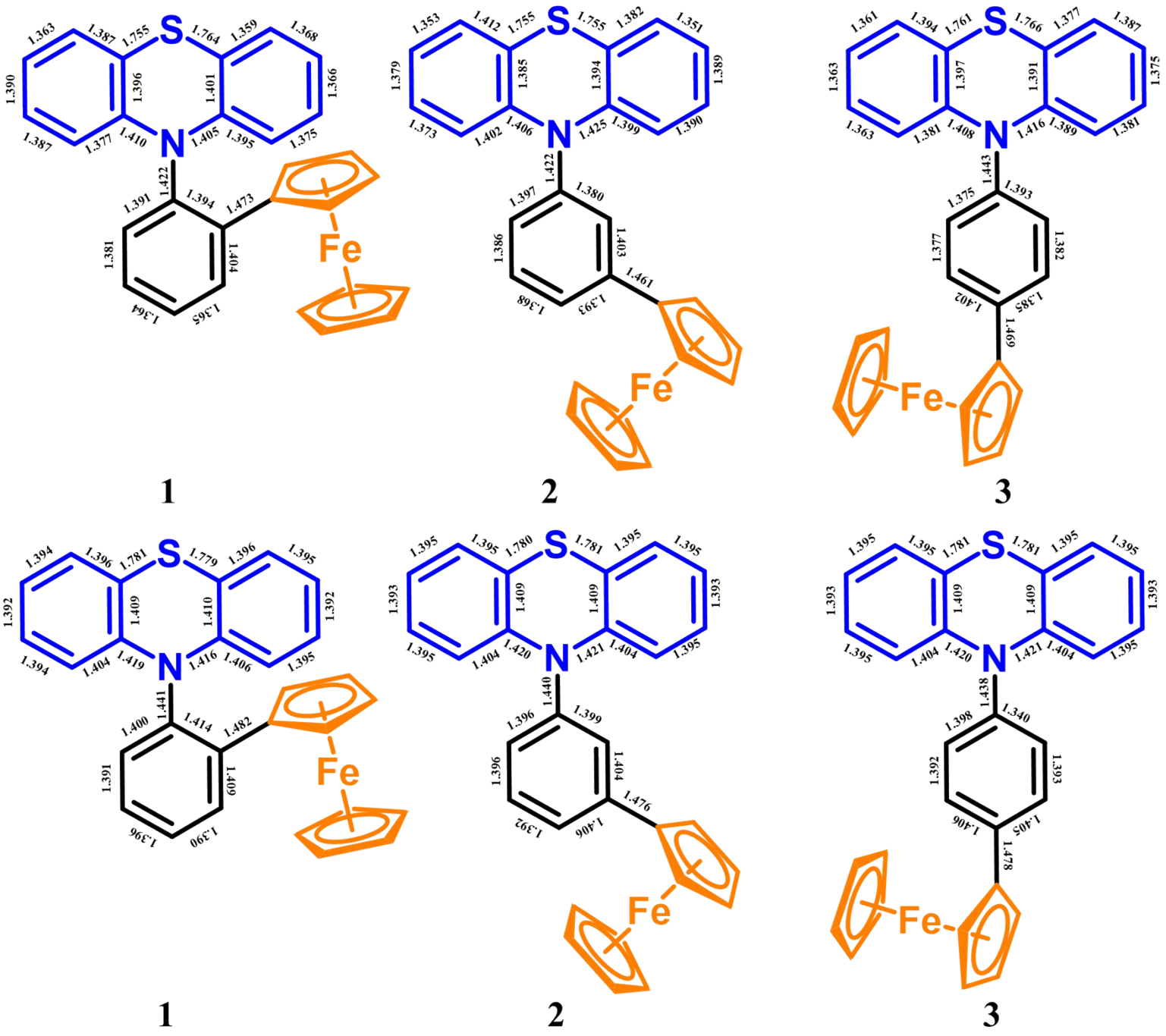

Fig. S20. Comparison of selected bond lengths of the crystal structures (above) and DFT optimized structures (below) of the ferrocene functionalized phenothiazine derivatives **1–3**.

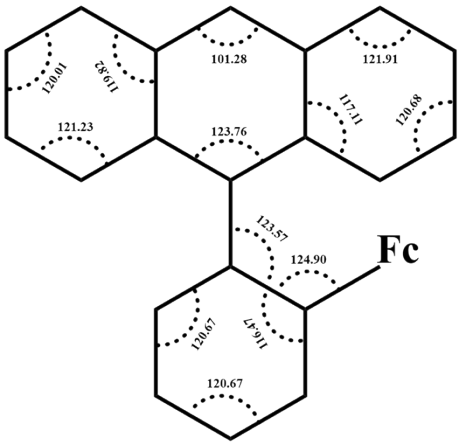
120.01
119.82
101.28
121.91
121.23
123.76
117.11
120.68
123.57
124.90
Fc
120.67
116.47
120.67

1

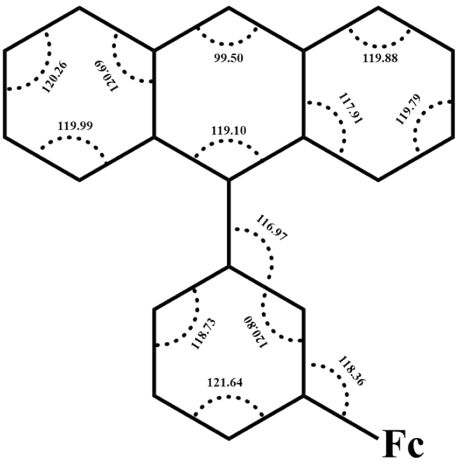
120.26
120.69
99.50
119.88
119.99
119.10
117.91
119.79
116.97
118.73
120.80
121.64
118.36
Fc

2

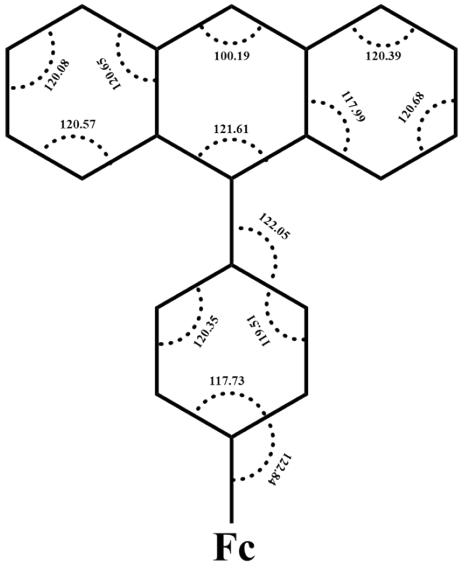
120.08
120.65
100.19
120.39
120.57
121.61
117.99
120.68
122.05
120.35
119.51
117.73
122.84
Fc

3

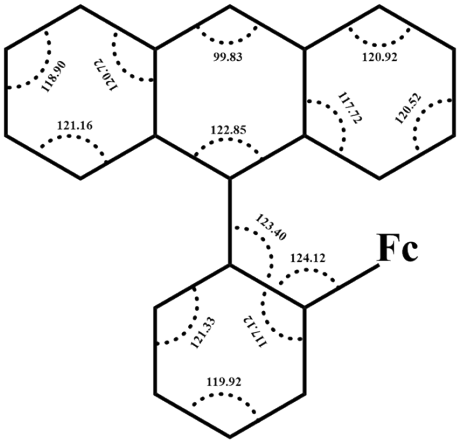
118.90
120.72
99.83
120.92
121.16
122.85
117.72
120.52
123.40
124.12
Fc
121.33
117.12
119.92

1

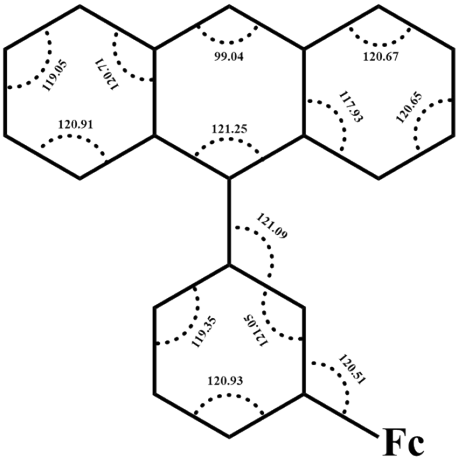
119.05
120.71
99.04
120.67
120.91
121.25
117.93
120.65
121.09
119.55
121.05
120.93
120.51
Fc

2

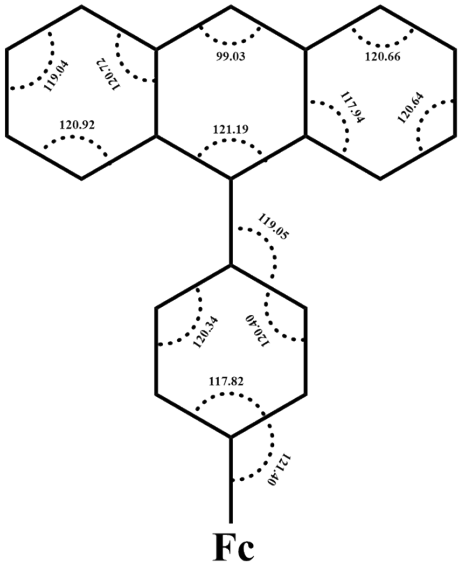
119.04
120.72
99.03
120.66
120.92
121.19
117.94
120.64
119.05
120.34
120.40
117.82
121.40
Fc

3

Fig. S21. Comparison of selected bond angles of the crystal structures (above) and DFT optimized structures (below) of the ferrocene functionalized phenothiazine derivatives **1–3**.

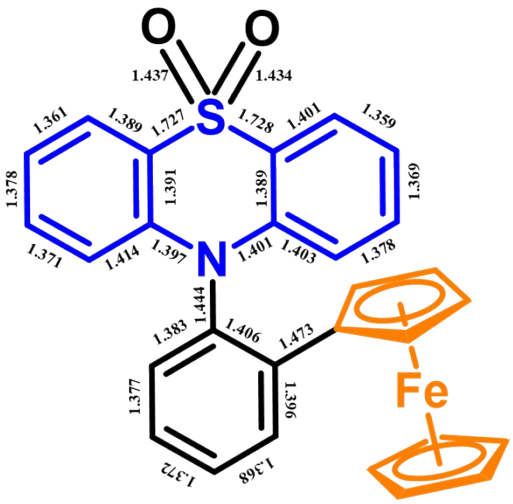
O
O
1.437
1.434
S
1.727
1.728
1.361
1.389
1.401
1.359
1.378
1.391
1.389
1.369
1.371
1.414
1.397
1.401
1.403
1.378
N
1.444
1.383
1.406
1.473
1.377
1.396
1.372
1.368
Fe

4

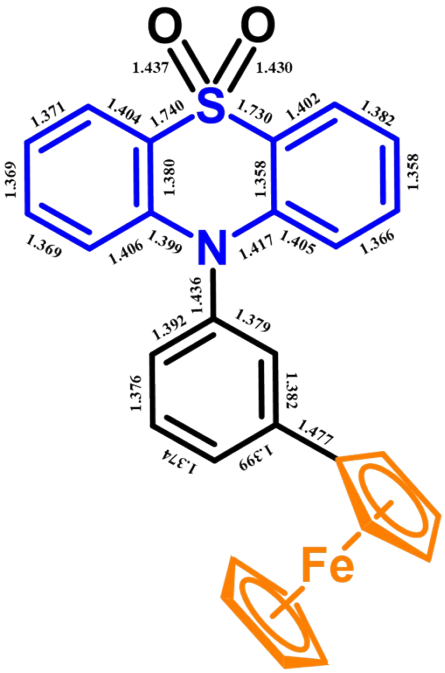
O
O
1.437
1.430
S
1.740
1.730
1.371
1.404
1.402
1.382
1.369
1.380
1.358
1.358
1.369
1.406
1.399
1.417
1.405
1.366
N
1.436
1.392
1.379
1.376
1.382
1.374
1.399
1.477
Fe

5

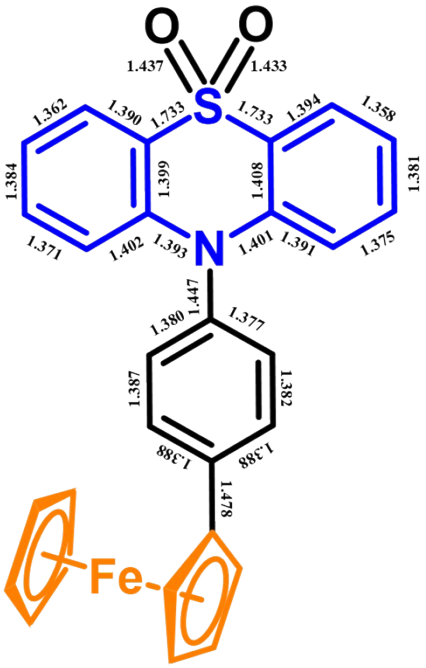
O
O
1.437
1.433
S
1.733
1.733
1.362
1.390
1.394
1.358
1.384
1.399
1.408
1.381
1.371
1.402
1.393
1.401
1.391
1.375
N
1.447
1.380
1.377
1.387
1.382
1.388
1.388
1.478
Fe

6

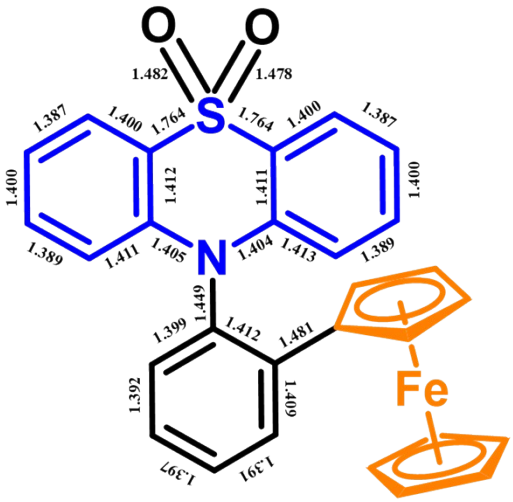
O
O
1.482
1.478
S
1.764
1.764
1.387
1.400
1.400
1.387
1.400
1.412
1.411
1.400
1.389
1.411
1.405
1.404
1.413
1.389
N
1.449
1.399
1.412
1.481
1.392
1.409
1.397
1.391
Fe

4

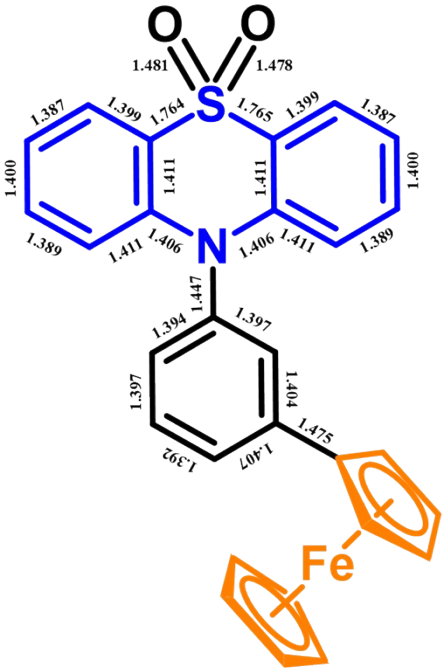
O
O
1.481
1.478
S
1.764
1.765
1.387
1.399
1.399
1.387
1.400
1.411
1.411
1.400
1.389
1.411
1.406
1.406
1.411
1.389
N
1.447
1.394
1.397
1.397
1.404
1.392
1.407
1.475
Fe

5

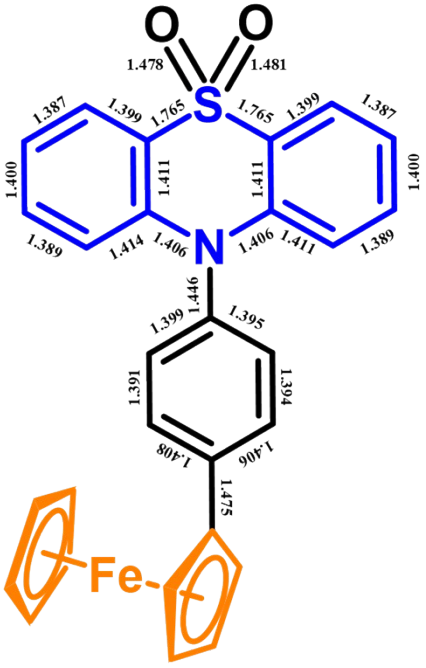
O
O
1.478
1.481
S
1.765
1.765
1.387
1.399
1.399
1.387
1.400
1.411
1.411
1.400
1.389
1.414
1.406
1.406
1.411
1.389
N
1.446
1.399
1.395
1.391
1.394
1.408
1.406
1.475
Fe

6

Fig. S22. Comparison of selected bond lengths of the crystal structures (above) and DFT optimized structures (below) of the ferrocene functionalized phenothiazine sulfone derivatives **4–6**.

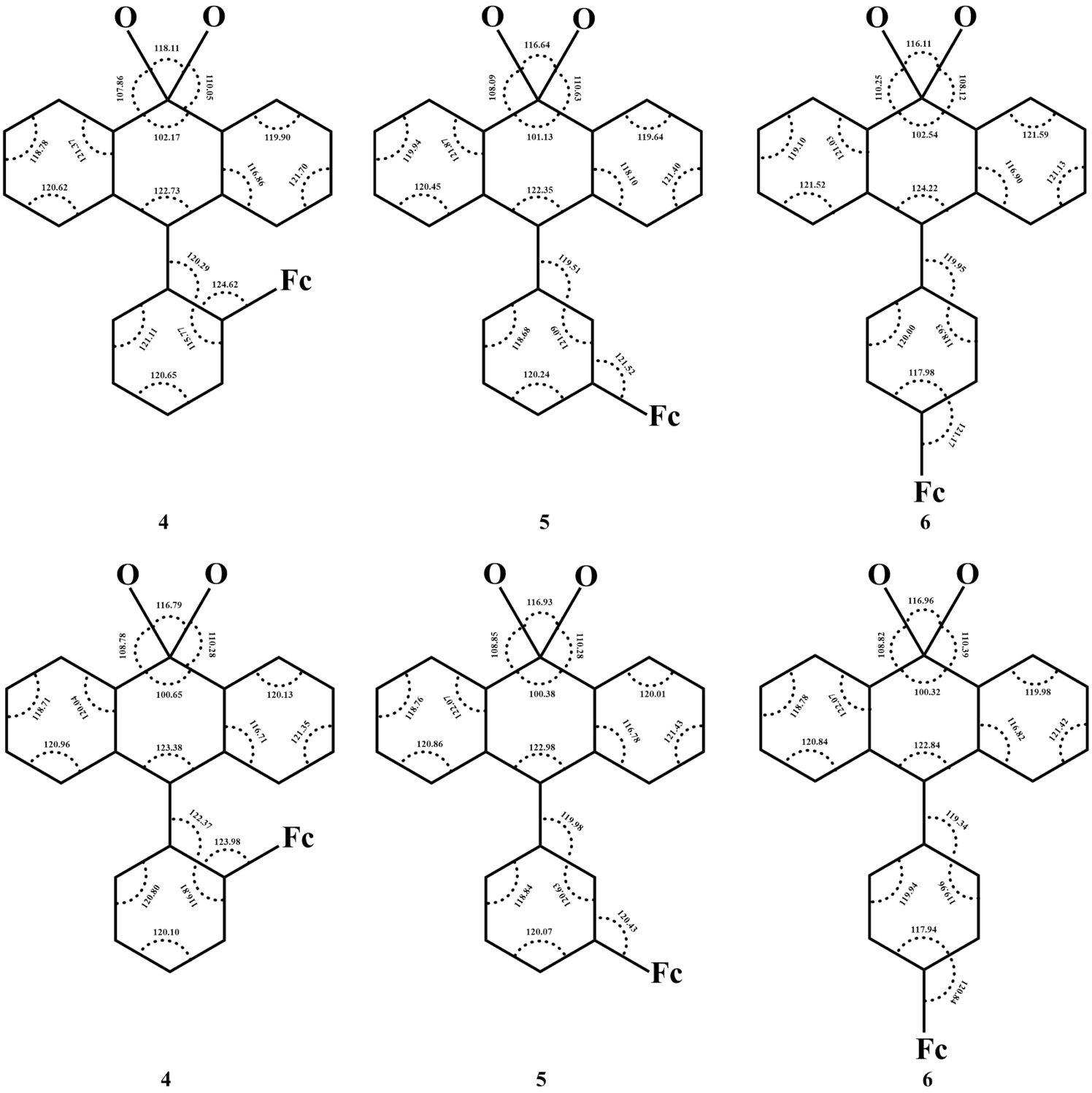

Fig. S23. Comparison of selected bond angles of the crystal structures (above) and DFT optimized structures (below) of the ferrocene functionalized phenothiazine sulfone derivatives **4–6**.

Density of State Analysis:

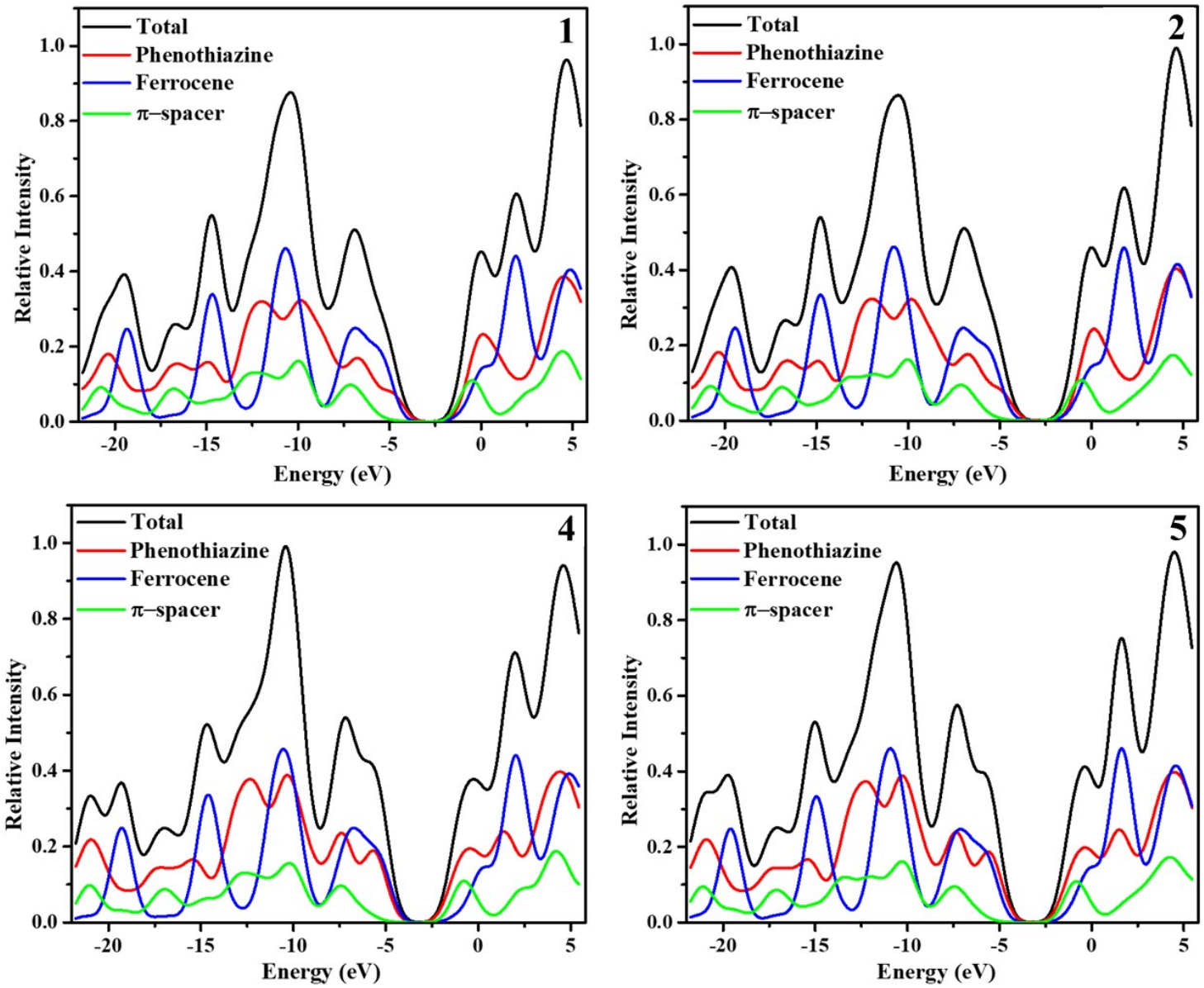

Fig. S24. Density of state (DOS) analysis of ferrocene functionalized phenothiazine and phenothiazine sulfone derivatives **1–2** and **4–5**.

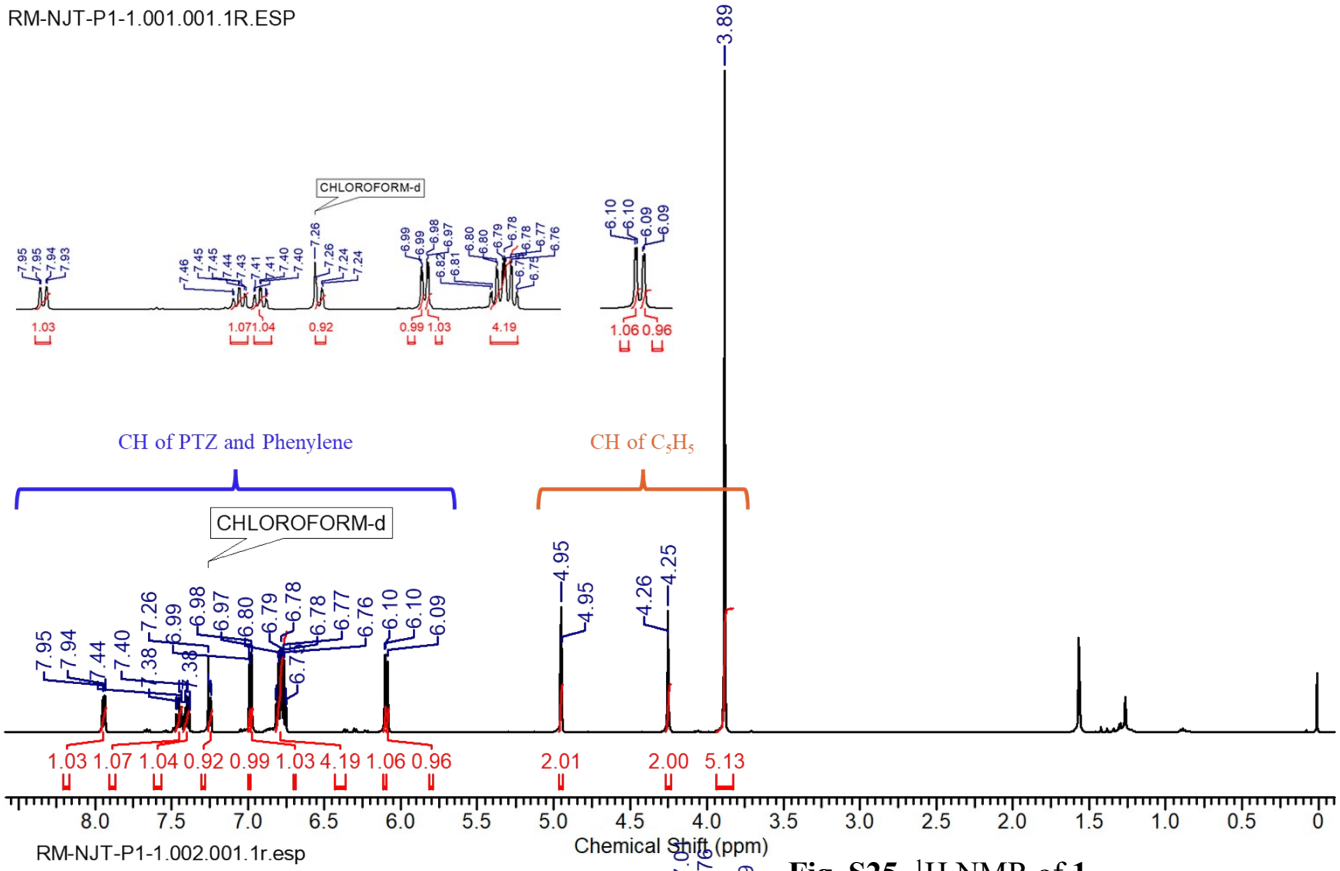

RM-NJT-P1-1.002.001.1r.esp

Fig. S25. ^{1}H NMR of **1**.

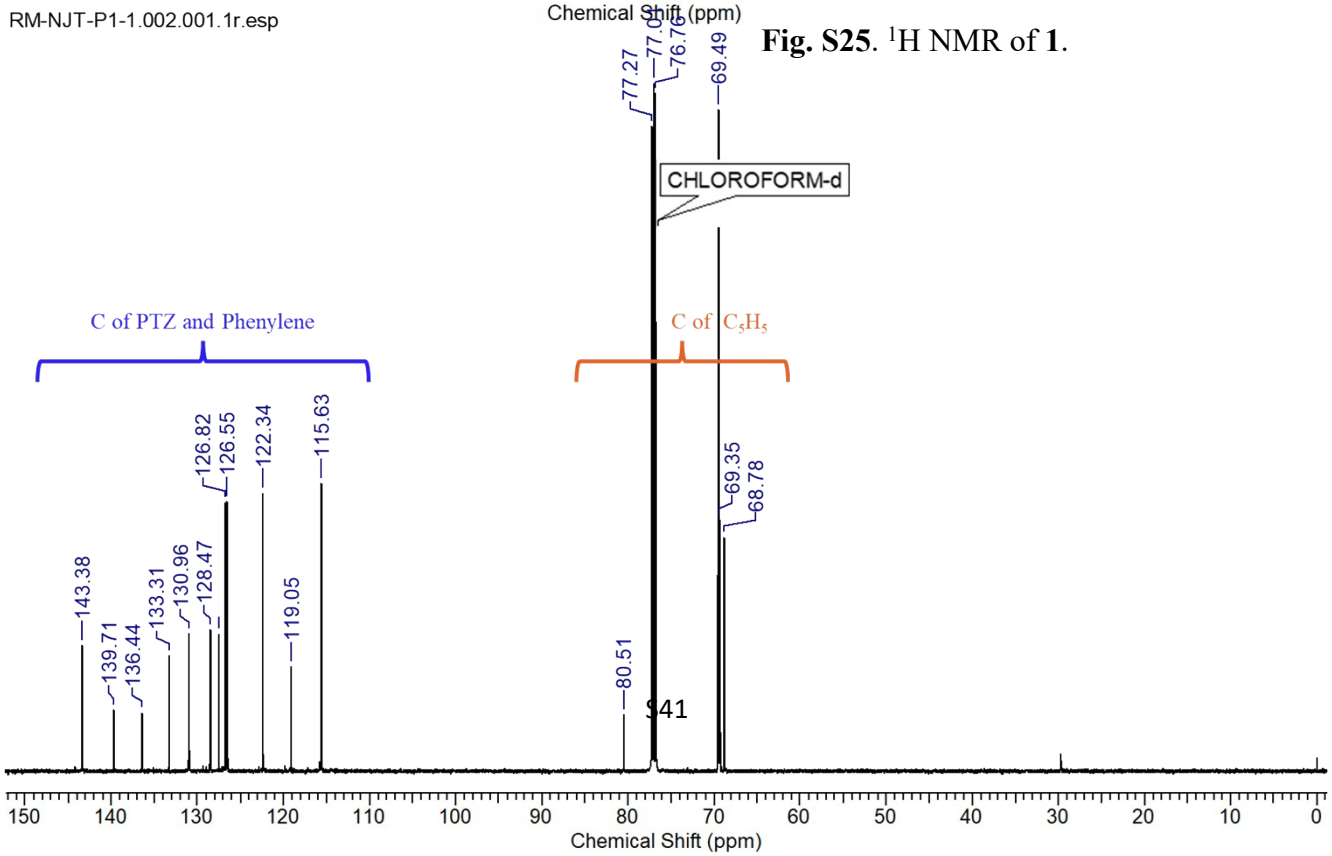

Fig. S26. ^{13}C NMR of **1**.

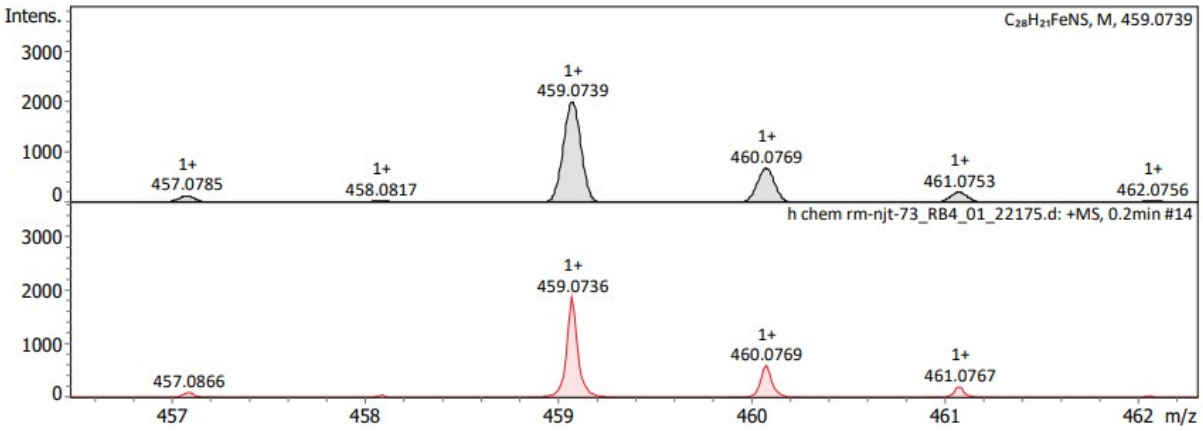

Fig. S27. HRMS of **1**.

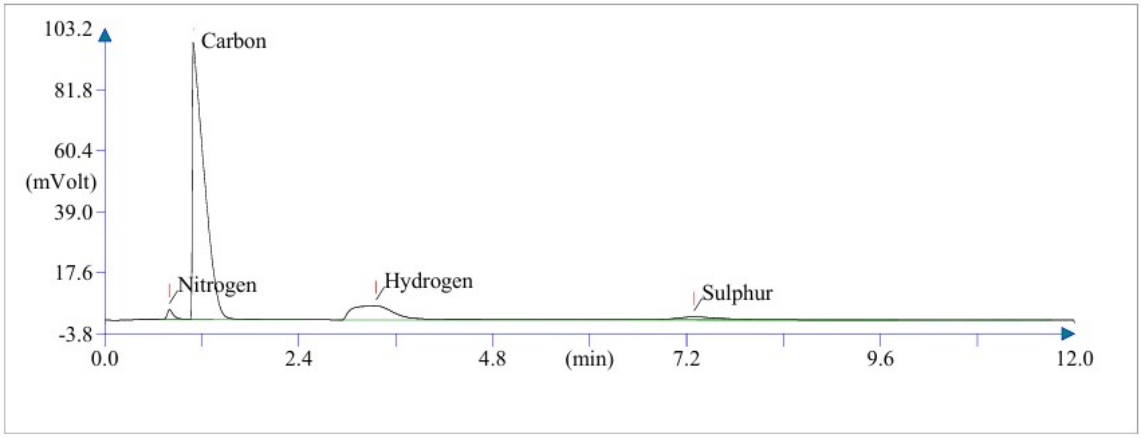

Operator ID:	
Company name:	ThermoFinnigan
Method filename:	C:\Eager for FLASH\04 JUL 24 CHNS\NCHS_19-12-2024.mth
Method name:	NCHS
Analysed:	22-01-25 13:18
Printed:	01-22-2025 15:07
Elemental Analyser method:	
Sampler method:	
Sample ID:	RM-NJT-PTZ1 (# 35)
Analysis type:	UnkNown
Chromatogram filename:	22-01-25-06.dat
Calibration method:	K Factors
Sample weight:	2.435
Protein factor:	6.25

Component Name	Element %	Retention Time (min)	Area (.1*uV*sec)
Nitrogen	3.032	0.800	190383
Carbon	72.915	1.092	9807700
Hydrogen	4.663	3.358	1886565
Sulphur	7.298	7.292	390373
	87.908		12275020

Fig. S28. Elemental analysis of **1**.

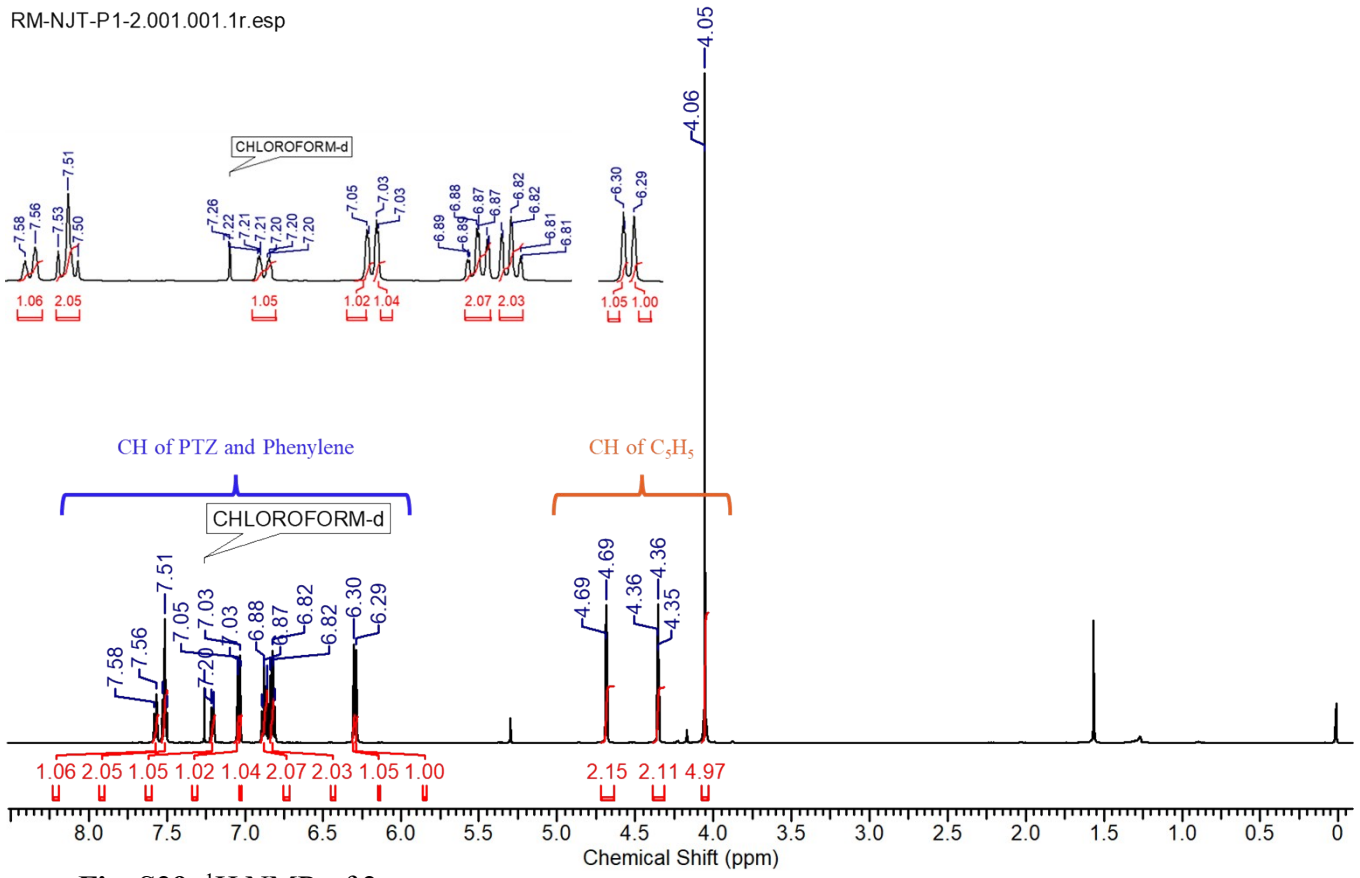

Fig. S29. ^{1}H NMR of **2**.

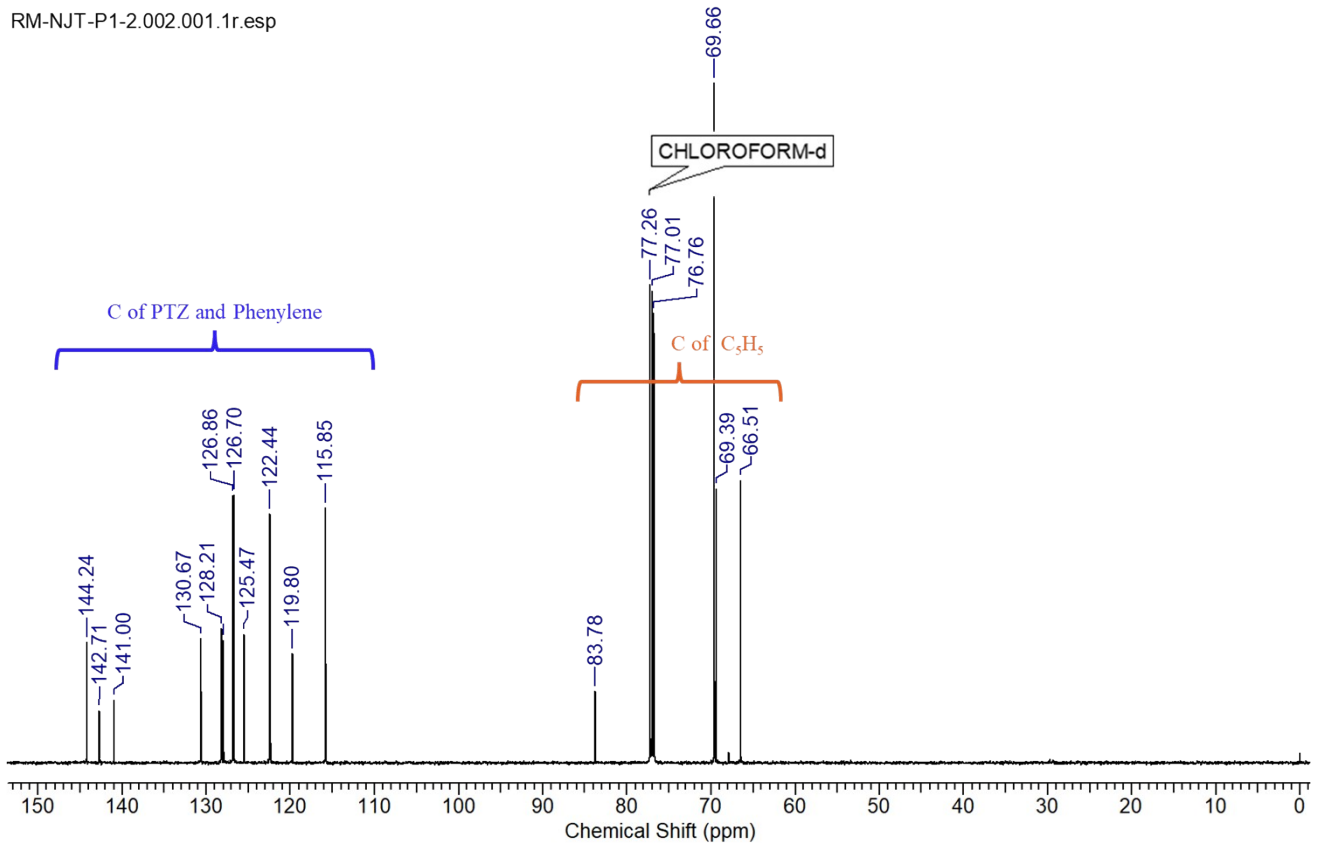

Fig. S30. ^{13}C NMR of **2**.

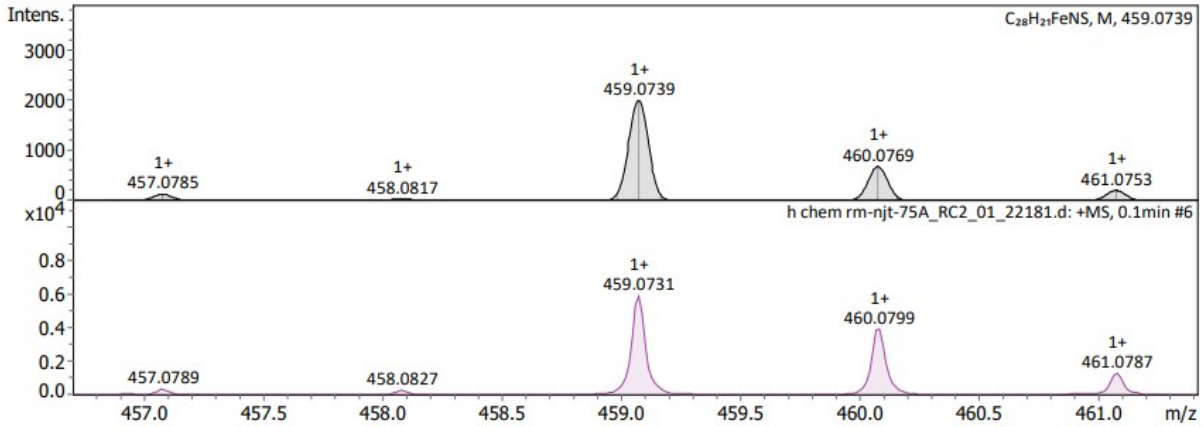

Fig. S31. HRMS of **2**.

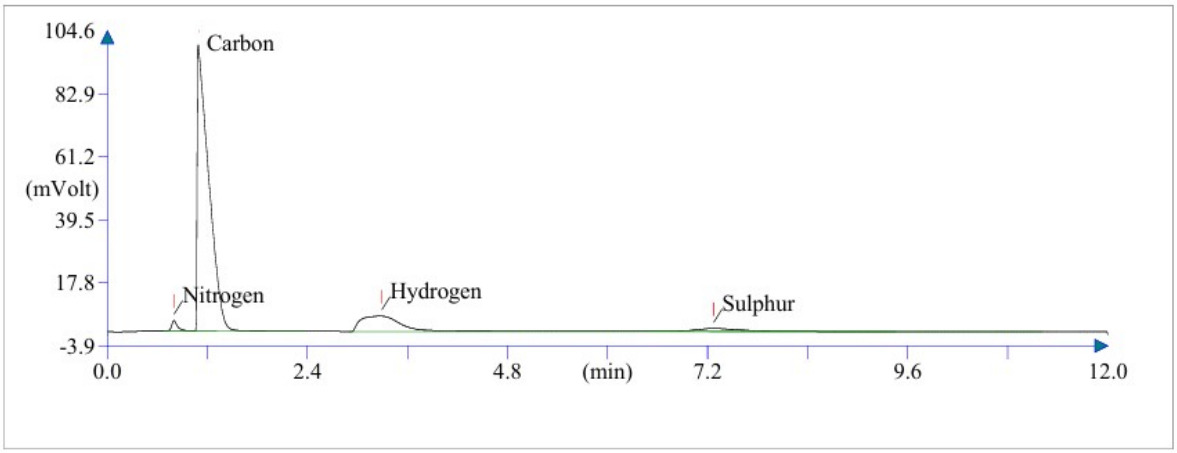

Operator ID:	
Company name:	ThermoFinnigan
Method filename:	C:\Eager for FLASH\04 JUL 24 CHNS\NCHS_19-12-2024.mth
Method name:	NCHS
Analysed:	22-01-25 13:43
Printed:	01-22-2025 15:08
Elemental Analyser method:	
Sampler method:	
Sample ID:	RM-NJT-PTZ2A (# 37)
Analysis type:	UnkNown
Chromatogram filename:	22-01-25-08.dat
Calibration method:	K Factors
Sample weight:	2.469
Protein factor:	6.25

Component Name	Element %	Retention Time (min)	Area (.1*uV*sec)
Nitrogen	2.845	0.800	182686
Carbon	69.832	1.092	9524390
Hydrogen	4.475	3.292	1835903
Sulphur	6.858	7.275	371937
	84.009		11914910

Fig. S32. Elemental analysis of **2**.

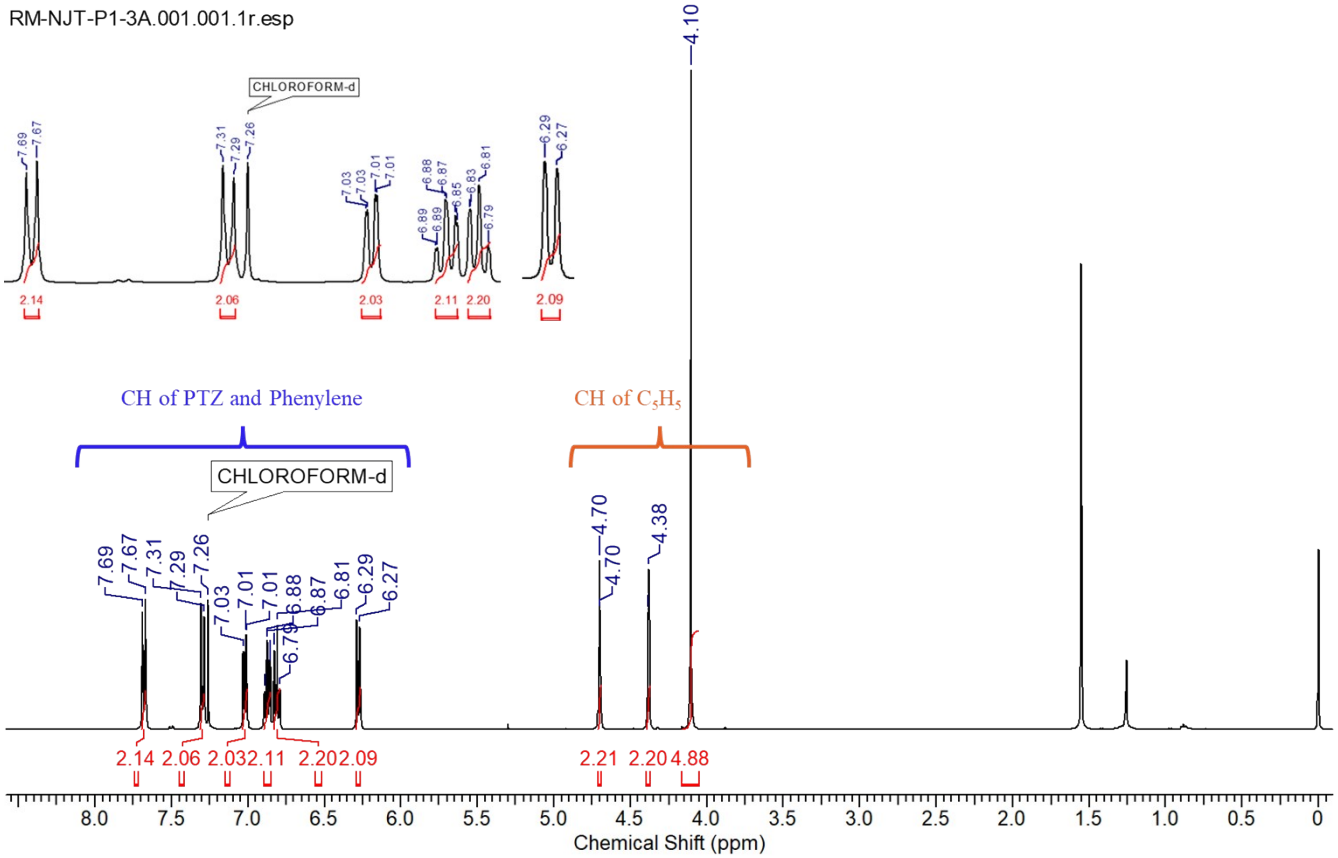

Fig. S33. ^{1}H NMR of **3**.

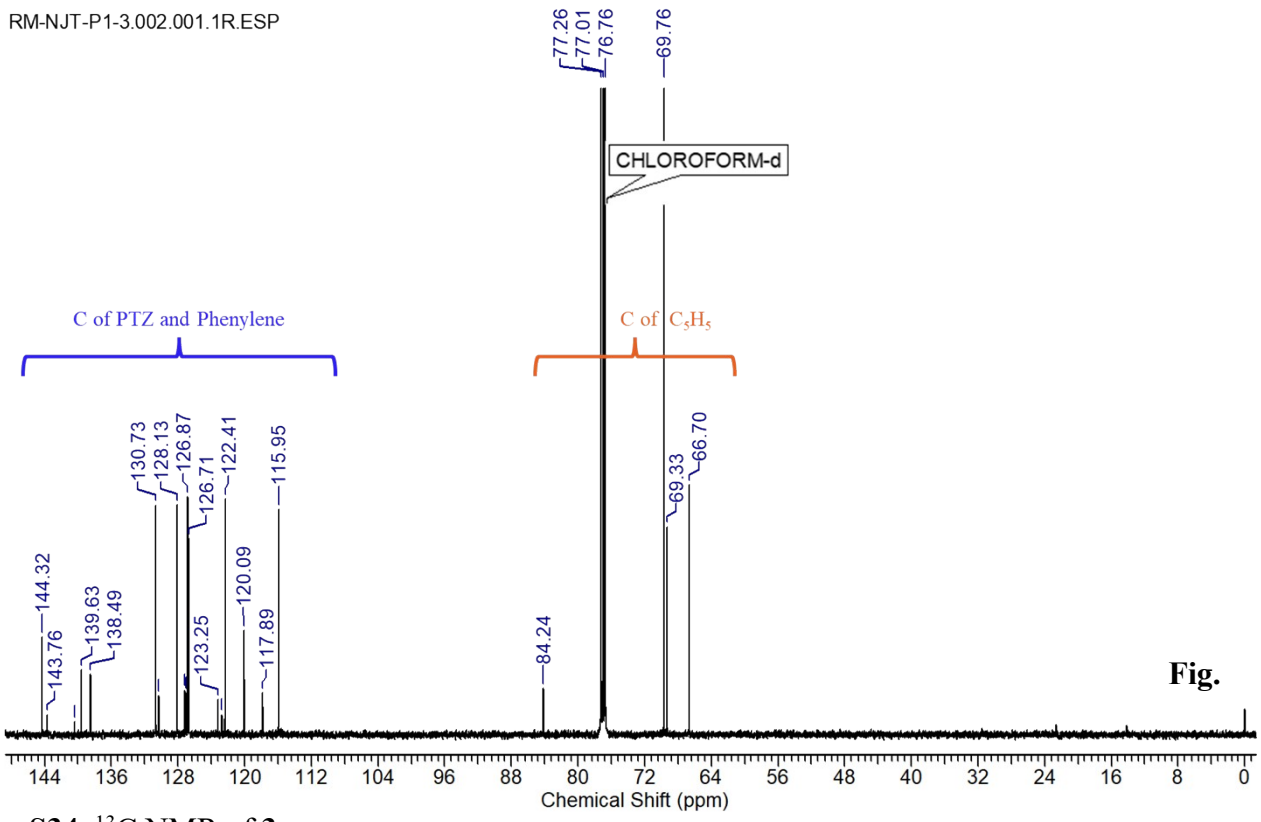

Fig. S34. ^{13}C NMR of **3**.

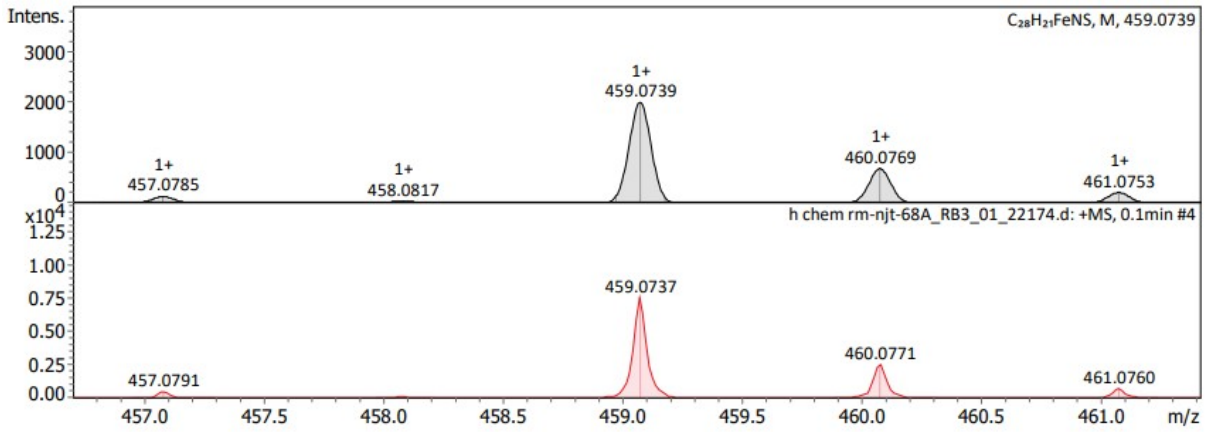

Fig. S35. HRMS of **3**.

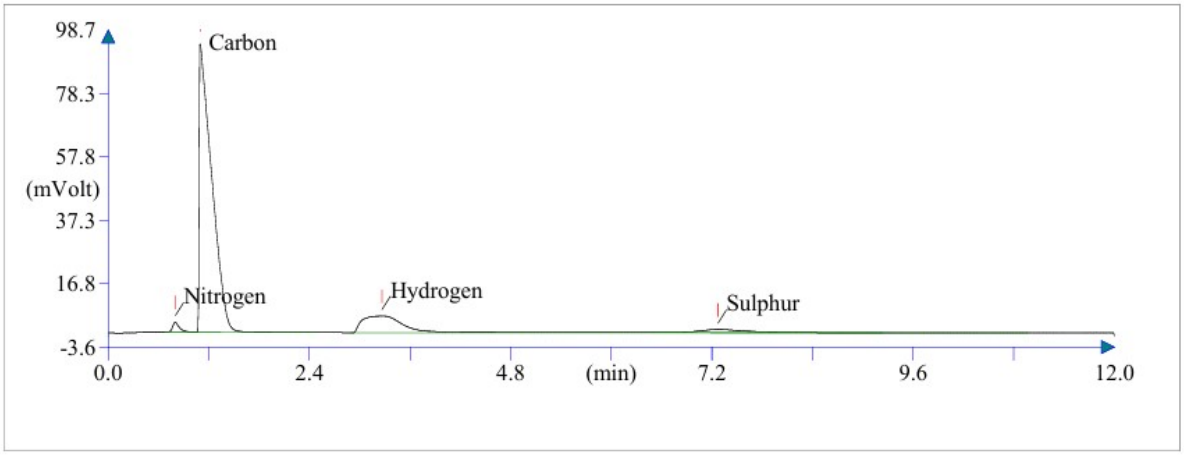

Operator ID:	
Company name:	ThermoFinnigan
Method filename:	C:\Eager for FLASH\04 JUL 24 CHNS\NCHS_19-12-2024.mth
Method name:	NCHS
Analysed:	22-01-25 13:55
Printed:	01-22-2025 15:08
Elemental Analyser method:	
Sampler method:	
Sample ID:	RM-NJT-PTZ3 (# 38)
Analysis type:	UnkNown
Chromatogram filename:	22-01-25-09.dat
Calibration method:	K Factors
Sample weight:	2.442
Protein factor:	6.25

Component Name	Element %	Retention Time (min)	Area (.1*uV*sec)
Nitrogen	2.923	0.800	185128
Carbon	71.970	1.100	9708501
Hydrogen	4.611	3.267	1870911
Sulphur	7.106	7.275	381207
	86.610		12145750

Fig. S36. Elemental analysis of **3**.

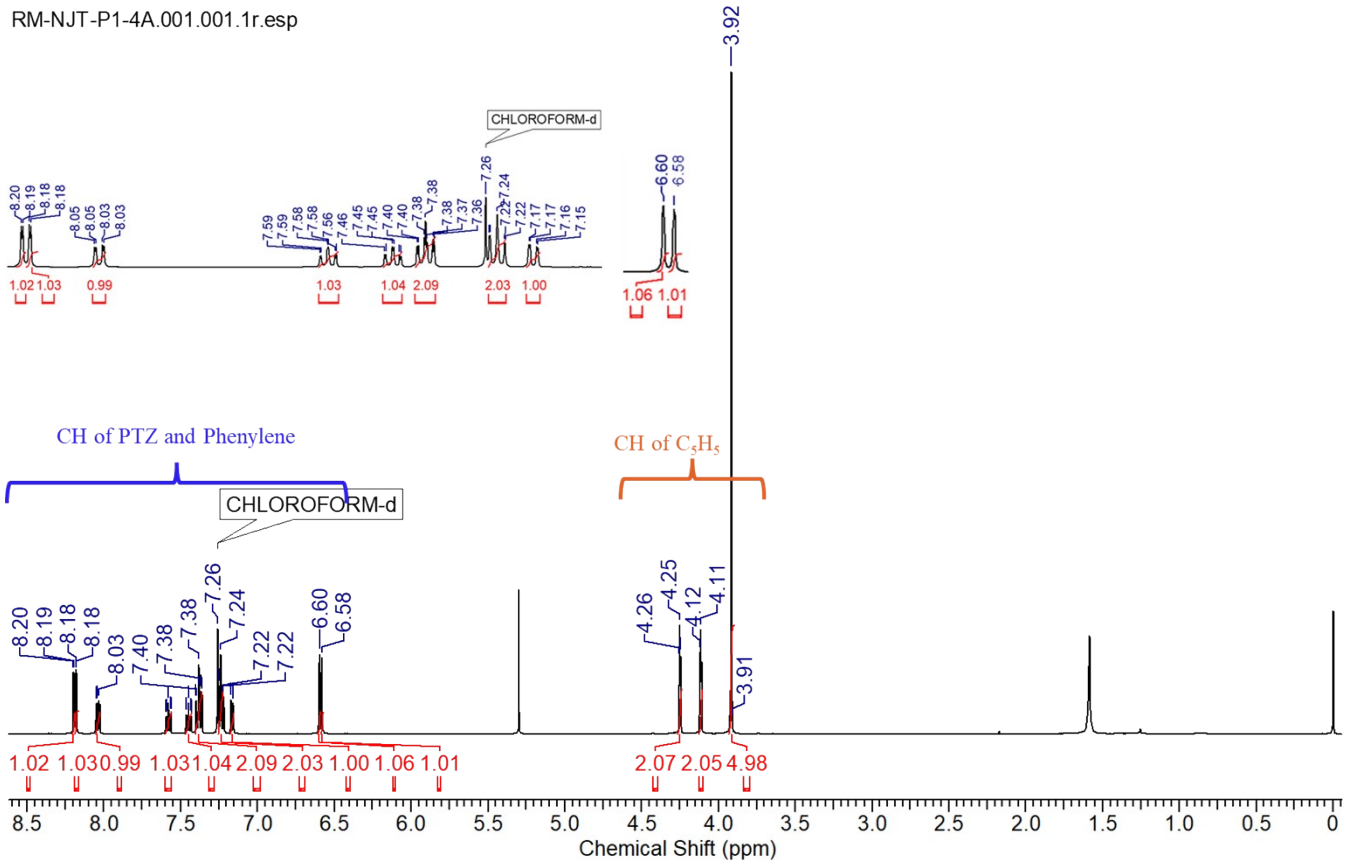

Fig. S37. ^{1}H NMR of **4**.

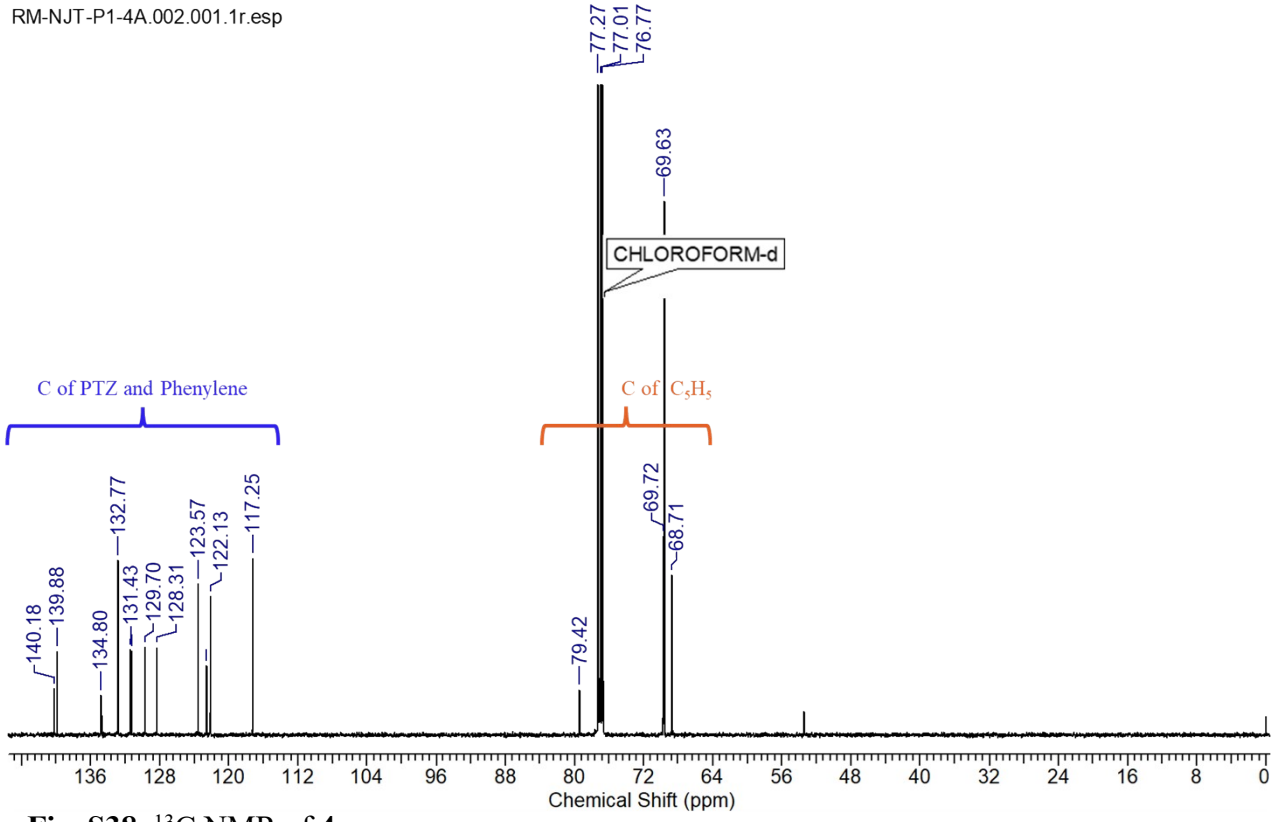

Fig. S38. ^{13}C NMR of **4**.

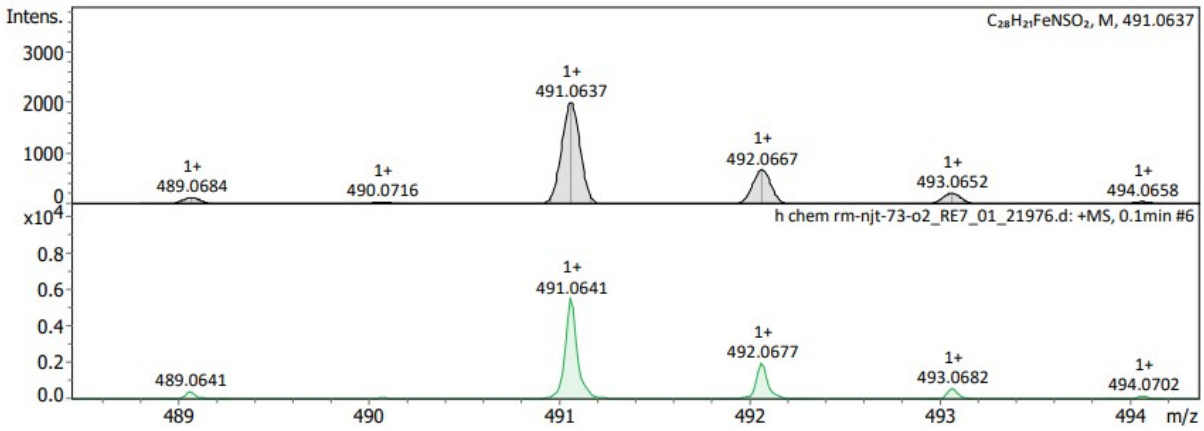

Fig. S39. HRMS of **4**.

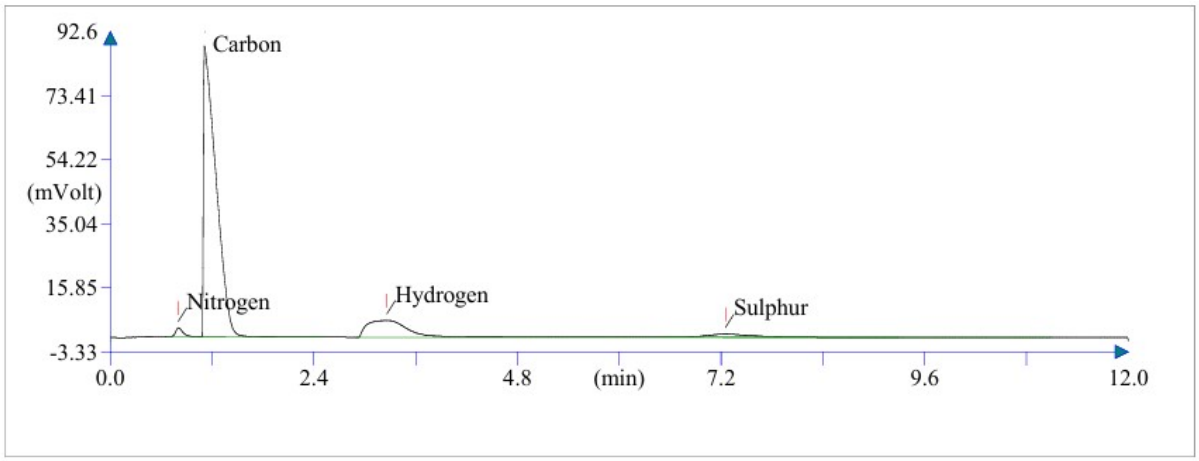

Operator ID:
Company name: ThermoFinnigan
Method filename: C:\Eager for FLASH\04 JUL 24 CHNS\NCHS_19-12-2024.mth
Method name: NCHS
Analysed: 22-01-25 14:53
Printed: 01-22-2025 15:09
Elemental Analyser method:
Sampler method:
Sample ID: RM-NJT-PTZ-A (# 42)
Analysis type: UnkNown
Chromatogram filename: 22-01-25-13.dat
Calibration method: K Factors

RM-NJT-P1-5A-001-001-1r.esp

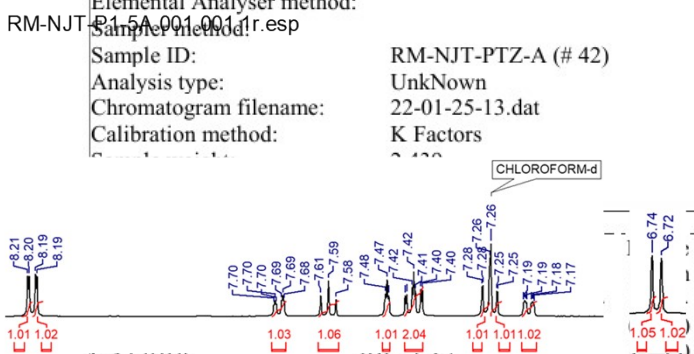

Hydrogen	4.302	3.258	1744054
Sulphur	6.500	7.250	348241
	79.539		11171770

Fig. S40. Elemental analysis of **4**.

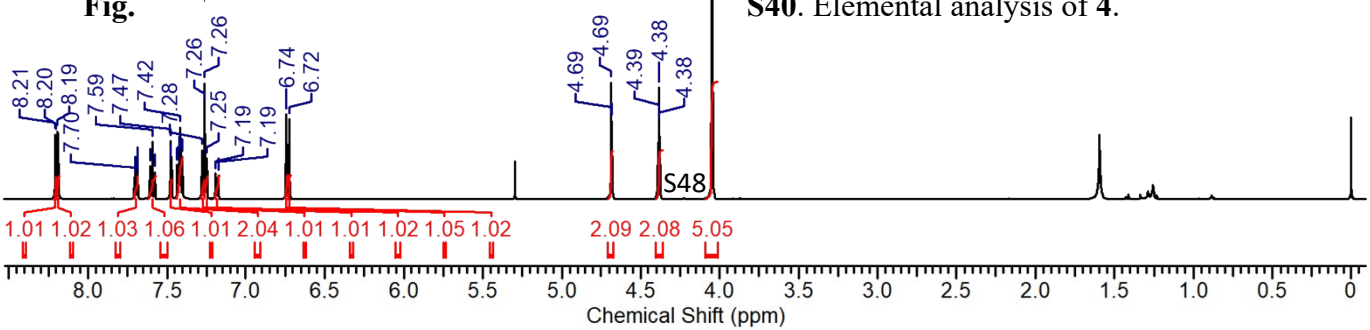

Fig. S41. ^{1}H NMR of **5**.

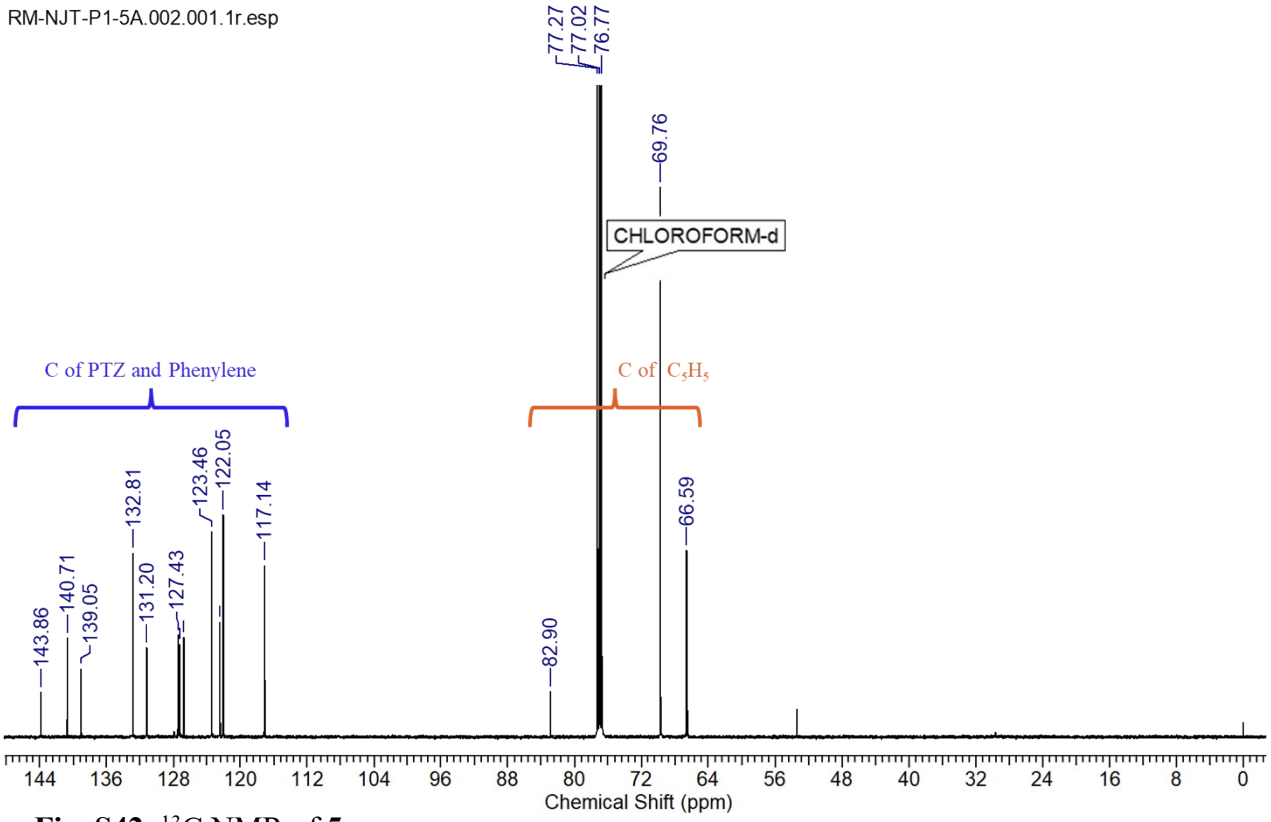

Fig. S42. ^{13}C NMR of **5**.

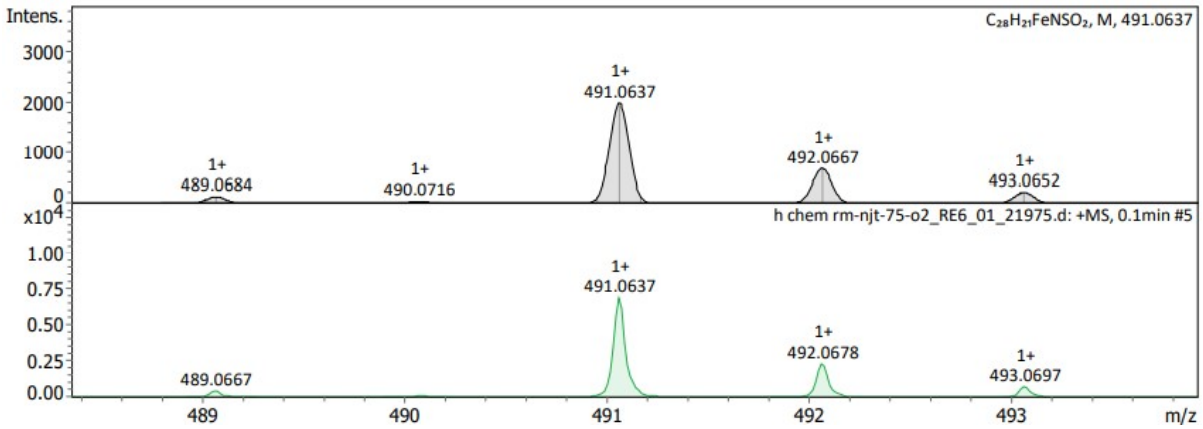

Fig. S43. HRMS of **5**.

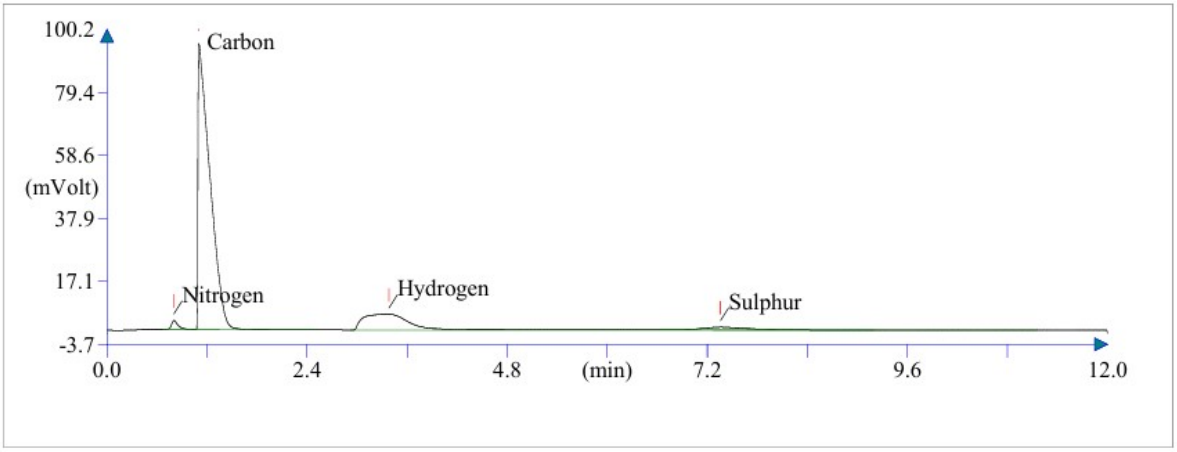

Operator ID:
Company name: ThermoFinnigan
Method filename: C:\Eager for FLASH\04 JUL 24 CHNS\NCHS_19-12-2024.mth
Method name: NCHS
Analysed: 22-01-25 14:26
Printed: 01-22-2025 15:08
Elemental Analyser method:
Sampler method:
Sample ID: RM-NJT-PTZ5 (# 40)
Analysis type: UnkNown

RM-NJT-P1-6A 001 001 1r.esp

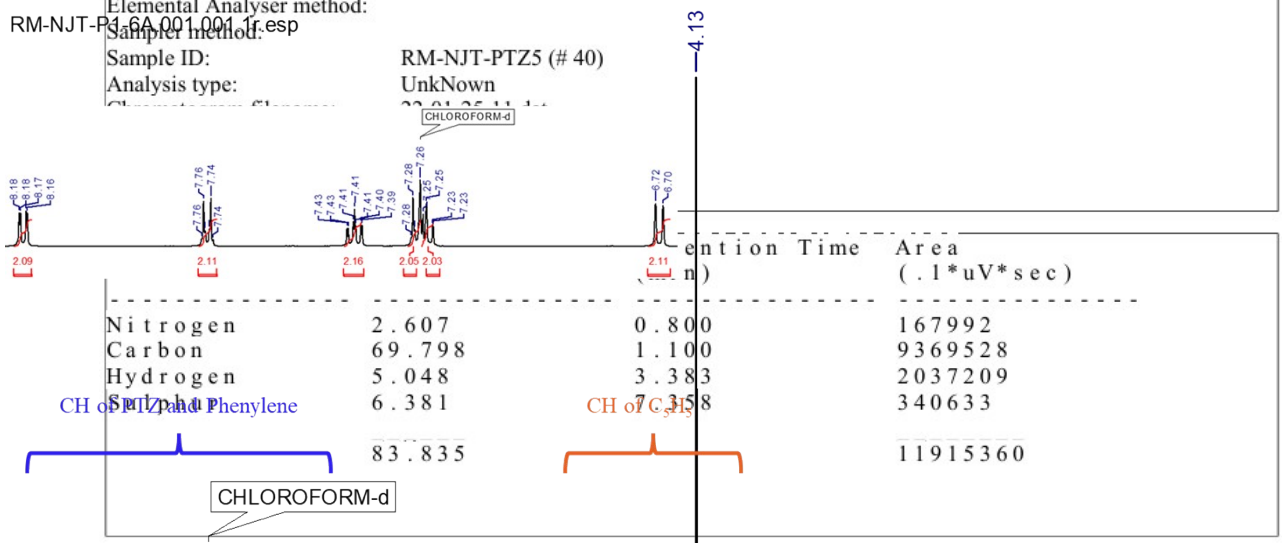

		ention Time n)	Area (.1*uV*sec)
Nitrogen	2.607	0.800	167992
Carbon	69.798	1.100	9369528
Hydrogen	5.048	3.383	2037209
Sulphur	6.381	7.358	340633
	83.835		11915360

CH of PTZ and Phenylene
CH of C_3H_5
CHLOROFORM-d

Fig. S44. Elemental analysis of **5**.

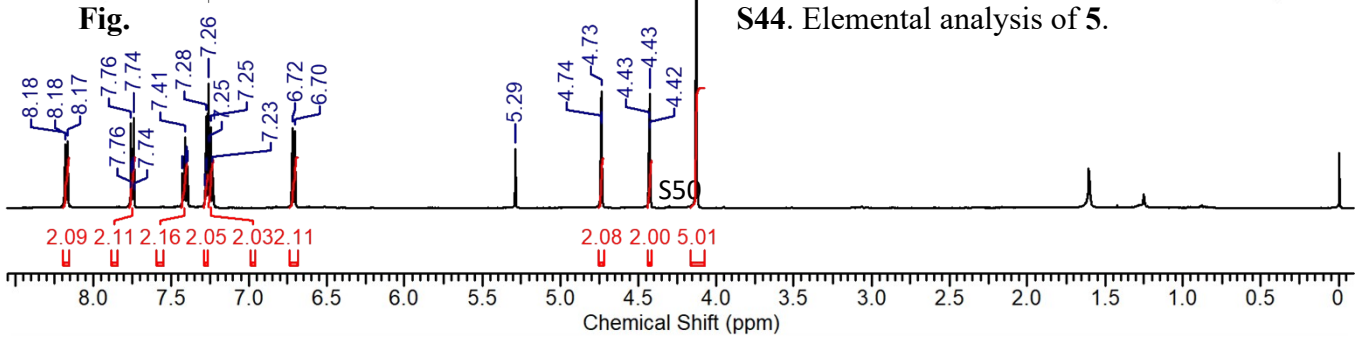

Fig. S45. ^{1}H NMR of **6**.

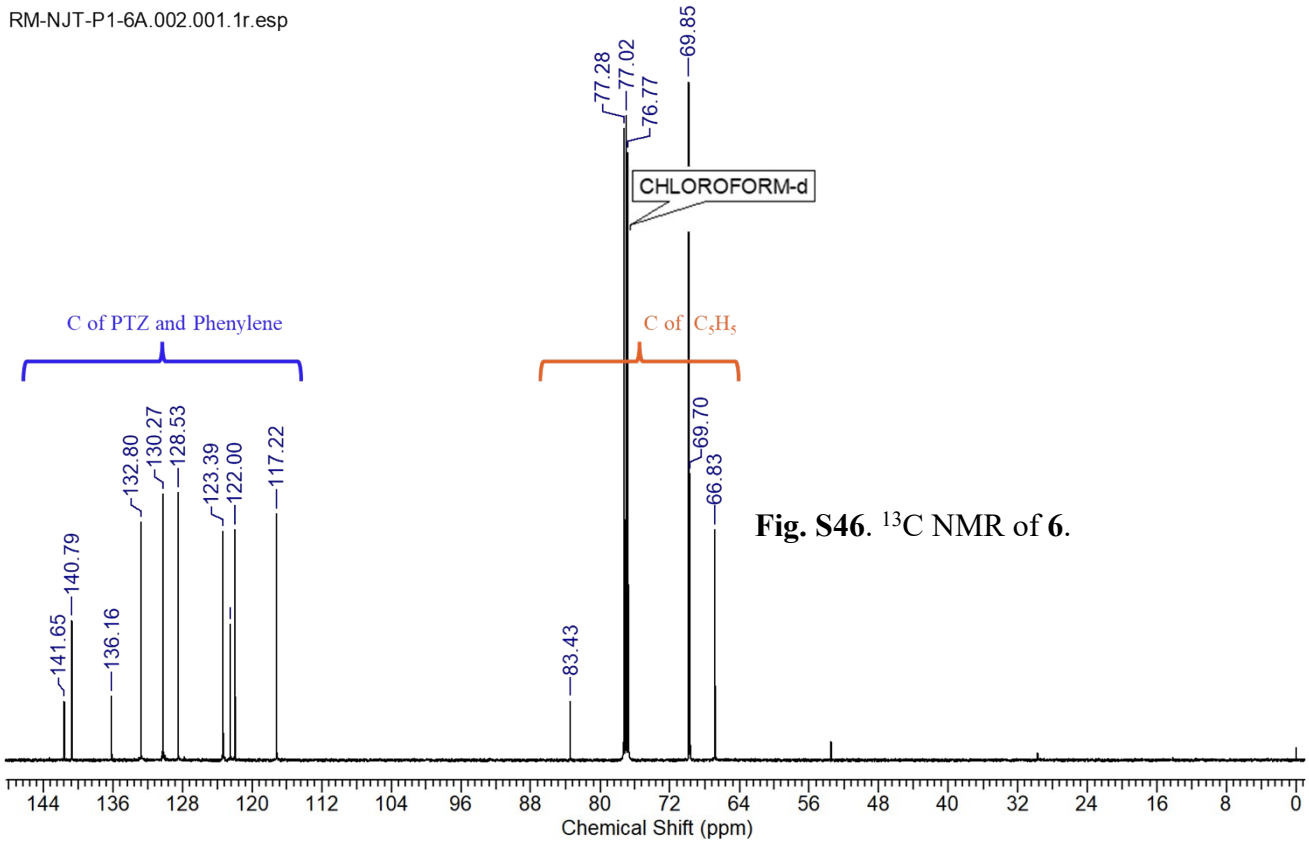

Fig. S46. ^{13}C NMR of **6**.

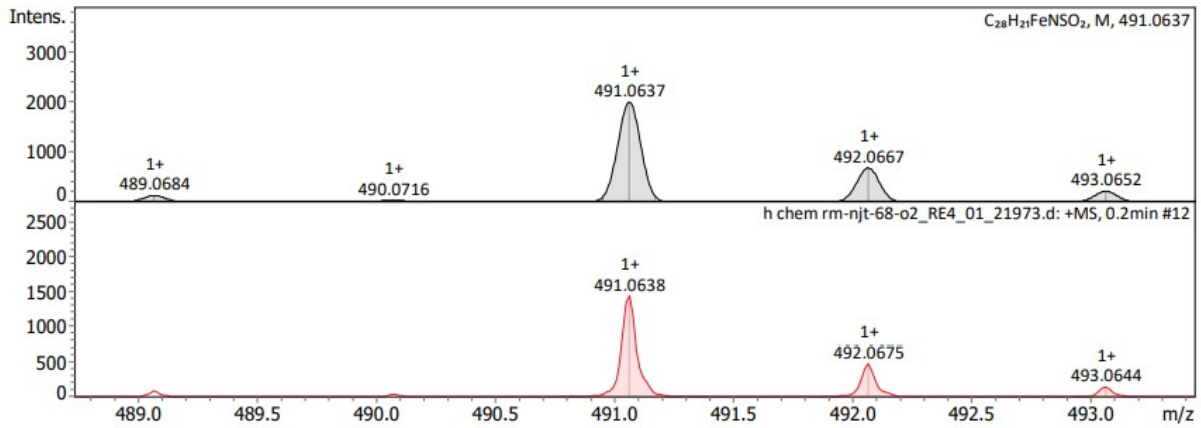

Fig. S47. HRMS of **6**.

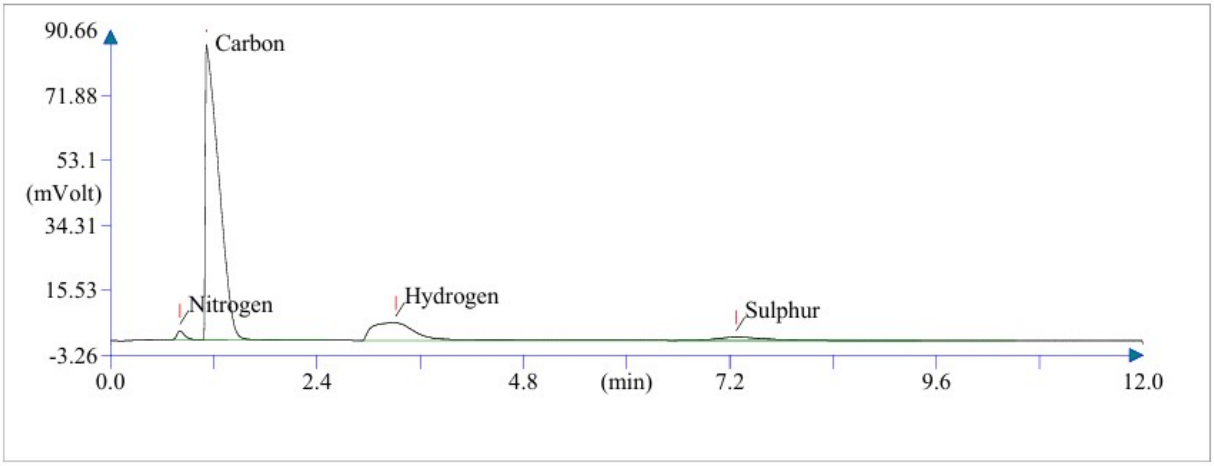

Operator ID:	
Company name:	ThermoFinnigan
Method filename:	C:\Eager for FLASH\04 JUL 24 CHNS\NCHS_19-12-2024.mth
Method name:	NCHS
Analysed:	22-01-25 14:38
Printed:	01-22-2025 15:09
Elemental Analyser method:	
Sampler method:	
Sample ID:	RM-NJT-PTZ6 (# 41)
Analysis type:	UnkNown
Chromatogram filename:	22-01-25-12.dat
Calibration method:	K Factors
Sample weight:	2.498
Protein factor:	6.25

Component Name	Element %	Retention Time (min)	Area (.1*uV*sec)
Nitrogen	2.617	0.808	172315
Carbon	67.220	1.117	9276024
Hydrogen	4.419	3.317	1834313
Sulphur	6.569	7.275	360440
	80.825		11643090

Fig. S48. Elemental analysis of **6**.

References:

1. Gaussian 09, Revision 09 W, M. J. Frisch, G. W. Trucks, H. B. Schlegel, G. E. Scuseria, M. A. Robb, J. R. Cheeseman, G. Scalmani, V. Barone, B. Mennucci, G. A. Petersson, H. Nakatsuji, M. Caricato, X. Li, H. P. Hratchian, A. F. Izmaylov, J. Bloino, G. Zheng, J. L. Sonnenberg, M. Hada, M. Ehara, K. Toyota, R. Fukuda, J. Hasegawa, M. Ishida, T. Nakajima, Y. Honda, O. Kitao, H. Nakai, T. Vreven, J. A. Montgomery, Jr., J. E. Peralta, F. Ogliaro, M. Bearpark, J. J. Heyd, E. Brothers, K. N. Kudin, V. N. Staroverov, R. Kobayashi, J. Normand, K. Raghavachari, A. Rendell, J. C. Burant, S. S. Iyengar, J. Tomasi, M. Cossi, N. Rega, J. M. Millam, M. Klene, J. E. Knox, J. B. Cross, V. Bakken, C. Adamo, J. Jaramillo, R. Gomperts, R. E. Stratmann, O. Yazyev, A. J. Austin, R. Cammi, C. Pomelli, J. W. Ochterski, R. L. Martin, K. Morokuma, V. G. Zakrzewski, G. A. Voth, P. Salvador, J. J. Dannenberg, S. Dapprich, A. D. Daniels, Farkas, J. B. Foresman, J. V. Ortiz, J. Cioslowski, D. J. Fox, Gaussian, Inc. Wallingford CT, 2009.
2. O. V. Dolomanov, L. J. Bourhis, R. J. Gildea, J. A. K. Howard, H. Pusch-mann, *J. Appl. Crystallogr.* 2009, **42**, 339–341.
3. G. M. Sheldrick, *Acta Crystallogr.* 2015, **71**, 3–8.
4. G. M. Sheldrick, *Acta Crystallogr.* 2008, **64**, 112–122.